Assessing Non-Rainfall Moisture Sources Through Relative Humidity and Soil Moisture in Dryland Regions

by

Desmond Andrew Hanan

A Thesis Presented in Partial Fulfillment
of the Requirements for the Degree
Master of Science

Approved November 2021 by the
Graduate Supervisory Committee:

Elizabeth Trembath-Reichert, Chair
Jnaneshwar Das
Heather Throop

ARIZONA STATE UNIVERSITY

December 2021

ABSTRACT

Drylands make up more than 45% of the Earth's land surface and are essential to agriculture and understanding global carbon and elemental cycling. This thesis presents an analysis of atmospheric relative humidity (RH) and temperature (T) as they impact soil moisture and water content at two dryland sites. In particular, this thesis assesses the likelihood and impact of non-rainfall moisture (NRM) sources on dryland soils. This work also includes a discussion of the development and testing of a novel environmental sensing network, using custom nodes called EarthPods, and recommendations for the collection of future data from dryland sites to better understand NRM events in these regions. An analysis of weather conditions at two drylands sites suggest that nighttime RH is frequently high enough for NRM events to occur. Thesis results were unable to detect changes in soil water content based on historical weather data, likely due to instrument limitations (depth and sensitivity of soil moisture probes) and the small changes in soil moisture during NRM events. However, laboratory tests of EarthPod soil moisture sensors indicated strong sensitivity to T. Characterization of these T sensitivities provide opportunities to calibrate and correct soil moisture estimates using these sensors in the future. This work provides the foundation for larger biogeochemical sampling campaigns focusing on NRM in dryland systems.

TABLE OF CONTENTS

Page

CHAPTER Page

LIST OF TABLES

LIST OF FIGURES

Figure Page

CHAPTER 1

INTRODUCTION

Dryland Biogeochemistry

Drylands are defined by their aridity, but more specifically this aridity can be characterized by the ratio of precipitation to evapotranspiration (P/PET). This ratio gives a measure of the amount of water entering a system to the amount leaving and, as the ratio decreases, it indicates that the region experiences increasing aridity. The P/PET of dryland systems spans from dry subhumid areas (0.50 - 0.65) through semiarid (0.20 - 0.50), arid (0.05 - 0.020), and hyperarid (<0.05) (Safriel *et al.*, 2005). These regions cover ~45% of the Earth's surface (Prăvălie, 2016) and account for about one quarter of global soil organic carbon (Plaza *et al.*, 2018). Consequently, drylands play a key role in affecting the atmospheric CO_2 pool at both interannual and decadal time scales (Poulter *et al.*, 2014; Ahlström *et al.*, 2015). Climate change projections estimate dryland area will increase 10% by the year 2100, with direct implications for food security and habitat stability (Plaza *et al.*, 2018).

Dryland ecosystems, particularly in North America, are uniquely heterogeneous in vegetative cover and soil texture in comparison to other ecosystems (Shreve *et al*. 1964; McAuliffe 1994). This varied pattern of shrub cover on submeter to meter scales and soil texture on meter to kilometer scales means that water dynamics, and even the microbial response to water pulses, can vary across submeter scales such as between a shrub canopy and a proximal interspace (Cable *et al*. 2008).

The Sonoran Desert, covering parts of southern Arizona, California and northern Mexico, ranges from semi-arid to hyper-arid conditions. Since the Sonoran Desert has

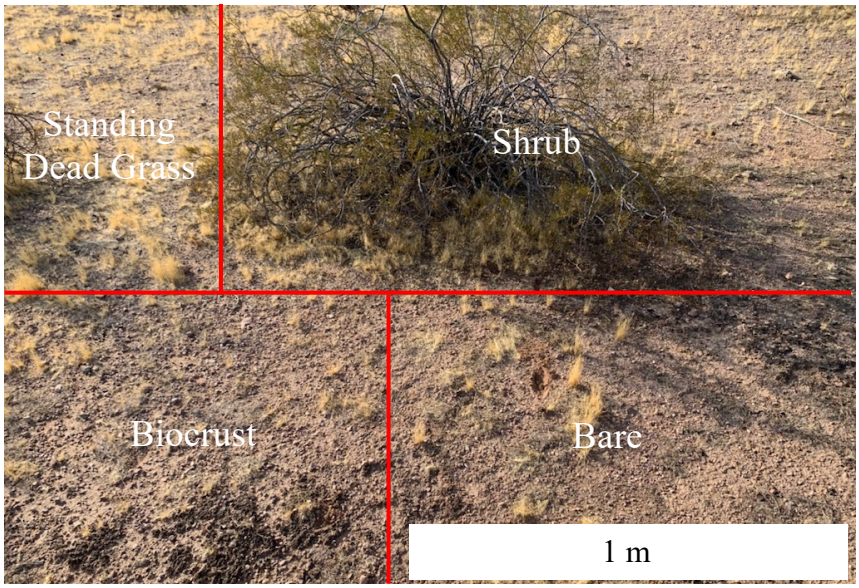

Figure 1: Shrub, standing dead grass, and a proximal bare plot with soil biocrust cover at the Tempe desert botanical garden demonstrating the heterogeneity of dryland microclimates on submeter scales.

about 30% plant cover (Shreve *et al*. 1964) and is, like other North American deserts, heterogeneous in soil texture (Cable *et al.* 2008), it is necessary to look at the different microclimates that bare soil and under canopy regions produce (Figure 1). For instance, previous bulk carbon (C), nitrogen (N), and sulfur (S) measurements indicate that under-canopy locations almost always have higher CNS concentrations due to an "island of fertility" effect (Mudrak *et al*. 2014), potentially correlating with increased litter retention in those areas.

Previous research on soil microbial communities has shown that microbes and moisture play a dominant role in soil biochemistry, carbon stabilization, litter decomposition and elemental cycling in drylands (Austin *et al*. 2004; Evans *et al.* 2020). Dryland soils contain approximately 25% of global soil organic carbon (Safriel *et al.*,

2005), and microbes play a role in both fixation of carbon and the mineralization of carbon substrates into CO_2 (Manzoni *et al.*, 2012). Similarly, drylands contain greater than 40% of global soil organic nitrogen (Plaza *et al.*, 2018) and soil moisture strongly regulates microbial response to nitrogen pools (Wertin *et al.*, 2018). Since microbial mineralization of soil organic matter is the primary source of inorganic soil nitrogen (Wang *et al.*, 2014), the pool of bioaccessible nitrogen available to plants in drylands is dependent on microbial activity. Similar to nitrogen, sulfur is both an essential nutrient for plant growth in the form of cysteine, methionine, coenzymes, and vitamins, and also a potentially limiting (Bünemann et al. 2007). Most previous research on microbial sulfur cycling in soil has focused on soil arylsulfatase (ARS) content. Since the vast majority of soil sulfur is organic, 90-98% (Scherer, 2001), the arylsulfatase enzyme, which catalyzes the formation of sulfate, has been a primary focus for research into microbial sulfur cycling (Chen *et al.*, 2019).

Water is a limiting factor for the growth, maintenance, and activity of microbes. To sustain themselves or perform more complex activities like elemental cycling, microbes must first acquire water. For this reason, most research on microbial activity in drylands has focused on their response to rainfall (Austin *et al*. 2004; Dirks *et al*. 2010; Evans *et al.* 2020). These events, however, tend to be short as soil dries rapidly post-rainfall, usually within a couple days or even hours (Huxman *et al*., 2004). During prolonged dry periods there may be other potential sources of moisture in dryland environments, such as fog, dew, soil water vapor adsorption, and mineral deliquescence (Wang *et al*. 2017, Davila *et al.* 2013, Canarini *et al.* 2020). These additional non-rainfall moisture (NRM) sources have been shown to stimulate microbial activity during rainless

periods (Kuehn *et al.* 2004, Evans *et al.* 2020, Dirks *et al.* 2010). Additionally, as aridity increases and rainfall decreases, NRM sources may become a more prominent portion of the total water budget. Therefore, NRM sources may have a profound impact on the frequency and duration of microbial activity, perhaps even more than rainfall, in arid and hyper-arid regions.

While characterization of moisture controls over soil microbial dynamics has typically focused on precipitation, non-rainfall moisture sources can also stimulate microbial metabolic activity in plant litter, biological soil crusts, and soils (Wang *et al.*, 2017). This activity includes respiration (Jacobson *et al.*, 2015; Gliksman *et al.*, 2017; Evans *et al.*, 2020) and carbon and nitrogen fixation (Ramond *et al.*, 2018; Ouyang and Hu, 2017). Furthermore, non-rainfall moisture manipulation experiments with dryland litter show that the microbial respiration response can be extremely rapid, with increased CO_2 production observed within minutes after non-rainfall moisture exposure in laboratory conditions (Jacobson *et al.*, 2015). Furthermore, it is possible that these microbial metabolic responses to NRM sources could differ significantly from responses to larger quantities of moisture such as during rainfall events. For example, certain elements of decomposition or nutrient cycling may have been prioritized during low moisture periods. Either way, the direct addition of even small amounts of liquid water immediately increases microbial access to substrates, rapidly increasing the microbial potential for decomposition and elemental cycling (Austin *et al.*, 2004).

Although microbial N cycling is typically modeled in association with rain events, RH changes may also activate microbial nitrogen fixation which creates larger reservoirs of nitrogen available to plants (Ramond *et al.*, 2018). The dynamics of ARS production

in dryland ecosystems is severely understudied (Bünemann *et al.,* 2007) and our understanding of how RH and NRM may affect soil S has yet to be studied. Bioavailable S is essential for plant growth and stoichiometrically coupled to C and N dynamics under most humidity regimes, but it can become decoupled in hyper arid conditions due to salinization and atmospheric deposition (Luo *et al.*, 2016). In these conditions, S oxidation can lead to decreased soil pH, enhanced solubility of trace metals, and associated shifts in the soil microbial community.

Sources and Measurement of NRM

Although fog and dew events are caused by separate phenomena, their impact on microbial soil communities is often assumed to be similar in models (Wang *et al.* 2017). A fog event occurs when atmospheric water vapor becomes saturated and condenses into small droplets suspended in the air (Figure 2). Dew, on the other hand, forms when the surface T of the soil or plant foliage is lower than the dewpoint, a T at which the water vapor in the air would be saturated (Jacobs *et al.* 1999). In both cases, water condenses at or near the soil surface and becomes available for microbial use (Figure 2).

Water vapor adsorption, on the other hand, occurs within the pores of the soil. When the atmospheric RH is higher than the soil RH, that gradient draws external water vapor into the pores of the soil where it can adsorb to the minerals and potentially form liquid water (Agam *et al.* 2006). This can occur at higher T than dew formation, which may also make it a more frequent source of water in dryland ecosystems.

Mineral deliquescence is another source of NRM that could be used by microbes as a moisture source in arid systems. When RH reaches the deliquescence relative

humidity (DRH) of a mineral, water vapor condenses on or in the pores of hygroscopic minerals causing the mineral to dissolve in on itself forming a brine or saturated solution (Davila et al 2013). While deliquescence can rely on water vapor adsorption to occur, the moisture source that microbes are accessing is a solution made up of the dissolution of the hygroscopic mineral and, therefore, has a decreased water activity relative to condensate.

	Dew	Fog	Water Vapor Adsorption	Mineral Deliquescence
Passive Collector	X	X		
Active Collector		X		
Leaf Wetness Sensor	X			
Soil Wetness Sensor	X		X	X
Microlysimeter	X		X	X
Soil Relative Humidity Sensor	X	X	X	X

Table 1: Ability of different methods of collection and sensing for assessing NRM event occurrence.

Each of these NRM sources can be measured in multiple ways (Table 1). Fog, for example, can be collected using both passive and active collectors to measure the quantity of moisture being deposited (Wang *et al.* 2017). Dew can also be measured directly using a variety of collectors that provide a surface on which dew can form. It is also possible to measure fog drip under canopies using passive collectors (Goodman 1985). Preliminarily, leaf wetness or soil wetness sensors can be used to determine when a moisture event is occurring on the surface or in the pores of soil, respectively. For

greater precision in quantity and length of an NRM event, microlysimeters are often used to calculate dewfall and water vapor adsorption (Ucles *et al.* 2013). However, because these NRM mechanisms all rely on RH, measuring soil and atmospheric RH may allow us to determine the length and extent of potential NRM events in these dryland systems. Previous research indicates that RH can be used to estimate when NRM events are occurring using either RH thresholds or functions to determine the 'likelihood wet' of a given soil system and humidity regime (Sentelhas *et al*., 2008; Evans *et al*., 2020).

RH is defined as the percent saturation of water vapor in the air at a given T. There are two potential environmental sources of increased soil RH in drylands that are both more likely to occur at night. Whenever the overlying air has a higher RH than the soil, water vapor in soil pores will increase as the soil equilibrates with the air (Agam *et al.*, 2006; McHugh *et al.*, 2015). However, this process is unlikely to occur during the daytime when soil T can be higher than the atmospheric T, creating a thermal gradient in the upper 5 cm that prevents soil RH from equilibrating (Kobayashi *et al.*, 1998; Pedram *et al.*, 2018). It is also possible that water vapor input from deeper, wetter soils can cause increase in the soil RH of surface soils; however, the same thermal gradient that prevents atmospheric water vapor penetration can also prevent deeper water vapor sources from entering the top 5 cm of the soil sometimes even creating a buildup of water vapor in the regions below the thermal gradient (Pedram *et al.* 2018). As soil T fall at night, dryland soil RH is more likely to increase and equilibrate with atmospheric input or even with vapor input from below.

Particularly in hotter regions, these conditions may lead certain types of NRM to be more frequent and more prevalent than others. Fog occurs during periods where water

vapor saturates the atmosphere (Figure 2) and, since percent saturation is inversely correlated with T, the conditions at which fog can occur are likely infrequent in most hot

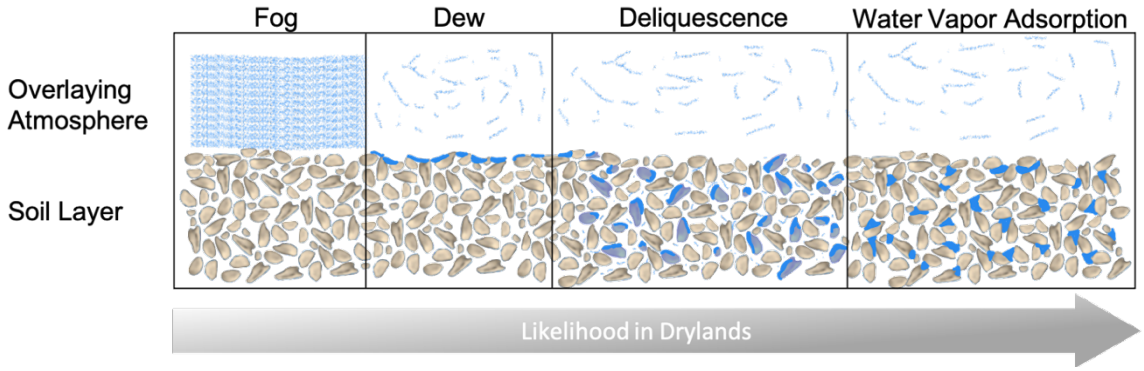

Figure 2: Illustration of different types of NRM and the conditions at which they occur against their likelihood to occur in dryland climate regimes. Fog conditions occur when the atmospheric RH reaches saturation. Dew occurs when the atmospheric RH is high and surface soil temperature is low, reaching the dewpoint. Similarly, deliquescence occurs when hygroscopic minerals experience soil or atmospheric RH reaching their deliquescent RH. And Soil water vapor adsorption occurs when the atmospheric RH is higher that the soil RH, creating a gradient moving water vapor into the pores of the soil.

climate regimes, although some cold deserts like the Atacama have significant fog input (Bonnail *et al.* 2018). Similarly, dew formation is dependent on low soil T and high RH (Figure 2) and may be more infrequent during hotter seasons. On the other hand, mineral deliquescence can occur whenever the soil RH is high enough (Figure 2) and, conversely, soil water vapor adsorption can occur whenever the soil RH is low enough in respect to the atmospheric RH (Figure 2) making both conditions potentially more likely to occur during dry seasons than other NRM sources.

This thesis focuses on determining the specific correlation of soil moisture and atmospheric and soil moisture measurements to determine if RH can be used as an accurate proxy for the occurrence of NRM events.

CHAPTER 2

CHARACTERIZATION OF SOIL MOISTURE IN RESPONSE TO ATMOSPHERIC VARIABLES

Introduction:

Since non-rainfall moisture (NRM) can stimulate a variety of microbial activities (Wang *et al.*, 2017; Jacobson *et al.*, 2015; Gliksman *et al.*, 2017; Evans *et al.*, 2020; Ramond *et al.*, 2018; Ouyang and Hu, 2017), it is important to determine the frequency, duration, and impact of NRM events in dryland regions. While fog and dew events are frequently predicted using dew point, previous research has indicated that it is possible to more broadly predict NRM occurrence using RH. In their 2020 paper discussing litter decomposition in the Namib Desert, Evans *et al*. found that a threshold of atmospheric RH sustained above 85% could be used to indicate NRM events. However, their research also indicated that, by correlating atmospheric RH measurements with leaf wetness sensor measurements, it was possible to closely model the frequency of NRM events over a given period. Since the Evans model uses leaf wetness sensors, it can only account for surficial NRM events like dew and fog and cannot account for other NRM soil events such as water vapor adsorption and deliquescence.

Here we use soil moisture sensors in conjunction with soil and atmospheric RH sensors to create a model that can predict NRM event occurrence in surface soils and, potentially, historical NRM event occurrence from data sets where soil moisture measurements are collected. These analyses are focused on soils in two contrasting sites in the Sonoran Desert in the southwestern USA (Figure 3). The Desert Botanical Garden (DBG) site contains remnant native desert patches characterized by arid desert scrubland

with coarse, gravelly soils in Phoenix, AZ at ~ 400 m elevation, predominated by *Larrea tridentata* shrubs (creosote bush). The Santa Rita Experimental Range (SRER) site is a semi-arid *Prosopis velutina* (mesquite) savanna near Tucson, AZ at ~ 1,100 elevation.

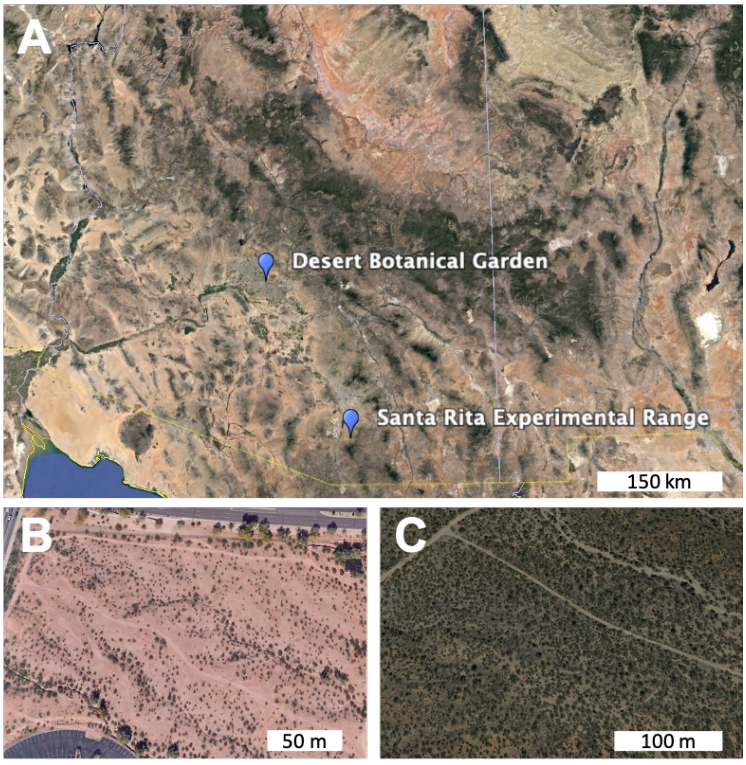

*Figure 3: **A)** Overview of southern Arizona, USA with the location of each site and close-up of **B)** arid Desert Botanical Garden and **C)** semi-arid Santa Rita Experimental Range sites.*

The SRER is a part of the National Ecological Observatory Network (NEON) and therefore has robust historical weather and soil data, in particular soil moisture, atmospheric RH and T, and rain data, accessible through NEON since 2016. The DBG, while not a part of NEON, has an onsite weather station run by Kevin Hultine that has collected rain, T, wind, and RH data since 2016 as well. In particular, the atmospheric RH and rainfall data from these two sites makes it possible to characterize the frequency at which elevated humidity occurs without rainfall events, when NRM events would be obscured, and determine if NRM events could be occurring. The soil moisture data from the SRER will also enable the comparison of soil water content with atmospheric RH to determine with greater specificity when NRM events could be occurring.

Methods:

Historical Weather and Soil Data Analysis

SRER NEON Data: Data including rain, soil moisture, dew point, atmospheric RH and atmospheric T were obtained from online NEON repositories (https://data.neonscience.org/data-products/explore). Soil VSWC data were not available or complete from these datasets before Jan. 2018 and after Jul. 2020. RH and T data from the SRER was collected using the Vaisala HUMICAP® HMP155 probe. At 2-meter height, this probe can measure RH from 0-95% with an uncertainty of 1% and T in a range of -80 to 60°C with an accuracy of at least 0.4°C. Volumetric soil water content (VSWC, cm^3 water/cm^3 soil) was measured using the Sentek TriSCAN EnviroSCAN soil moisture probe. Each probe was calibrated in an external laboratory by site and depth. The EnviroSCAN measures at multiple depths; however, to best determine how atmospheric variables impacted soil moisture, the sensor closest to the surface (6 cm depth, installed vertically) was used. At this depth, NEON reported a maximum uncertainty of 0.21 cm^3/cm^3 from Jan. 2018 – Apr. 2018 and 0.07 cm^3/cm^3 from Apr. 2018 – present.

DBG Data: Unpublished data from the DBG including rain, dew point, atmospheric RH and T were obtained directly from K. Hultine. Rain, RH, and T data are based on near surface (2 m above soil surface) sensors on an onsite meteorological station.

Data Analysis: NEON and DBG data were analyzed using both Microsoft Excel and MATLAB. Large data sets were solely analyzed in MATLAB. Both data sets were

processed and missing, incomplete, or potentially inaccurate data as indicated by NEON metadata were removed. Some RH, T, precipitation, and soil moisture data from the SRER was not processed. These data included RH, T and VSWC data from before 2018 and after July 2020, which was largely incomplete, and precipitation data from prior to 2018 which was also missing some data points. Fog and dew analyses were performed on the complete unfiltered data set remaining. To remove confounding variables for analyses of smaller NRM events, VSWC, T and RH data were filtered to remove rainy days (>0.05 mm precipitation). Linear regression models were performed using the MATLAB fitlm function (Math Works, Inc.).

Results:

Historical Weather Characterization of Sites

Given the importance of moisture events in dryland regions, we have endeavored to characterize the frequency and duration of moisture events at both sites and the typical conditions under which they occur. From 2019 and 2020, in keeping with the aridity of both locations, the SRER received significantly more precipitation than the DBG (Figure 4). Overall, 2020 was a drier year at both sites. Both sites saw an increase in precipitation during the winter months in both 2019 and 2020.

Heatmaps of historical weather records from both DBG and SRER show elevated atmospheric relative humidity occurs most frequently at lower atmospheric T (Figure 5). The DBG, an arid scrubland, is characterized by higher T and generally lower RH. Similarly, the semi-arid SRER has lower T on average and generally higher RH.

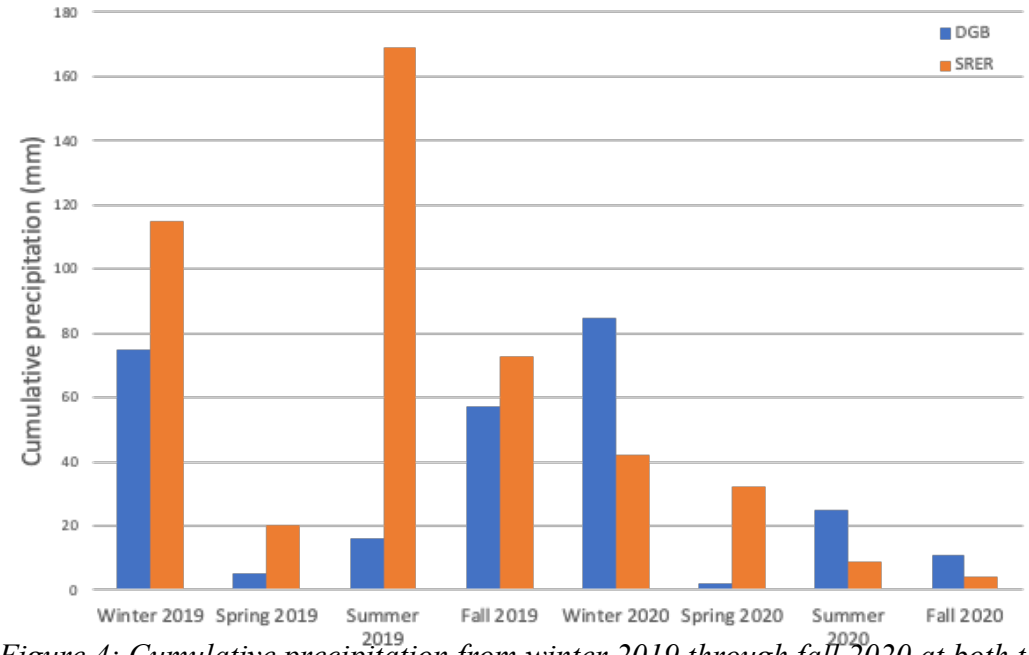

Figure 4: Cumulative precipitation from winter 2019 through fall 2020 at both the DBG (Blue) and the SRER (Orange). Seasons were ascribed as follows: Jan. – Mar. (Winter), Apr. – Jun. (Spring), Aug. – Sep. (Summer), and Oct. -Dec. (Fall).

Furthermore, over half the days in a year (50% of days at the DBG and 70% of days at the SRER) reached a maximum RH above 50% (Figure 6). Typically, periods of high RH occurred at nighttime and co-occurred with lower T. At the SRER and DBG respectively, the average T when the RH exceeds 75% is 11.1°C and 10.5°C. A fog or dew event may occur at each site, depending on wind conditions, if the dew point equals or exceeds the T. To estimate the frequency and duration of fog and dew at both sites, there were three potential thresholds by which to make estimates: a conservative threshold of dewpoint ≥ T, a semi-conservative threshold of dewpoint + 2.5 °C ≥ T, and a broader threshold of dewpoint + 4°C ≥ T (American Meteorological Society, 2020). The semi-conservative estimation was used to consider natural variation caused by other weather factors such as humid or cold winds, which can increase the likelihood of dew formation. Rainy days

were calculated to be any day with cumulative precipitation >0.005 mm. These analyses indicated that fog and dew events primarily occurred in winter seasons at the SRER, typically from late October through April (Figure 7). Further analyses indicated that, at the DBG, fog and dew conditions occurred most frequently at and in the hours before 6 am then trailed off rapidly to a low point around 1 pm (Figure 8A). At the SRER, however, fog and dew conditions occurred most frequently around 5 am, but otherwise followed the same general diurnal trend (Figure 8B).

As there were no soil moisture sensors at the DBG weather station, soil moisture data was only analyzed from the SRER from Jan. 2018 – Dec. 2020. While NEON provided data from deeper sensors, the soil moisture sensor data used was from the sensor placed closest to the surface at a depth of 6 cm. Rainy days were not excluded from this data set. The volumetric soil water content (VSWC) of the soil represents the amount of water in grams per gram of soil.

Analyses of this soil moisture data indicated that the soil at the SRER site equilibrated to a VSWC of approximately 0.02 cm^3/cm^3 during prolonged dry periods (Figure 7). Most large moisture events (> 0.02 cm^3/cm^3 above a VSWC of 0.02 cm^3/cm^3) occurred from Jul.–Oct. both years and less frequently during winter months from Nov. – Feb., potentially co-occurring with rainfall which also followed similar trends during those periods (Figure 4, 7).

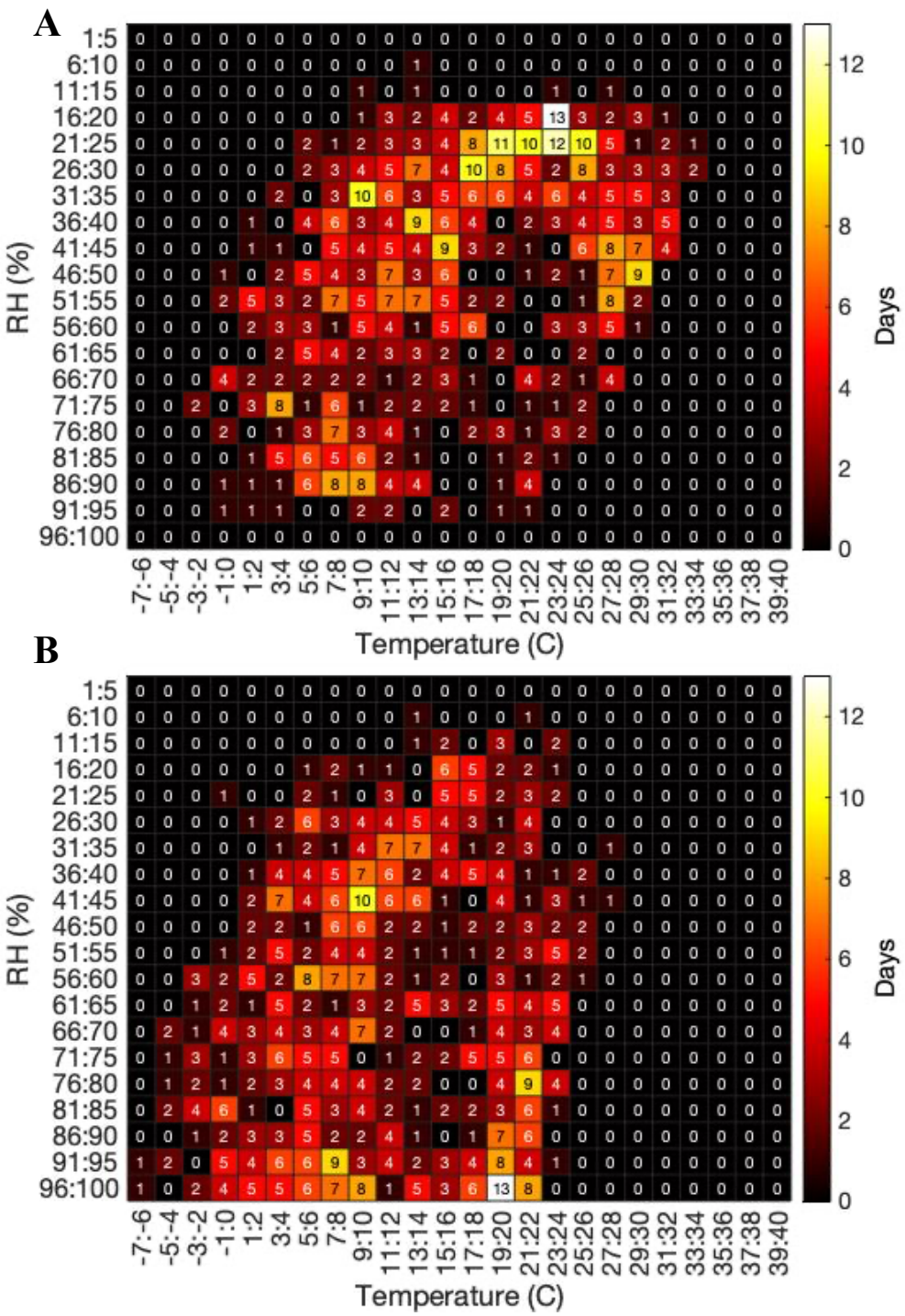

*Figure 5: Heatmaps of daily maximum RH against minimum T at the DBG (**A**) and SRER (**B**) from Jan. 2018 - Dec. 2019. Counts indicate the maximum RH and minimum T of each day.*

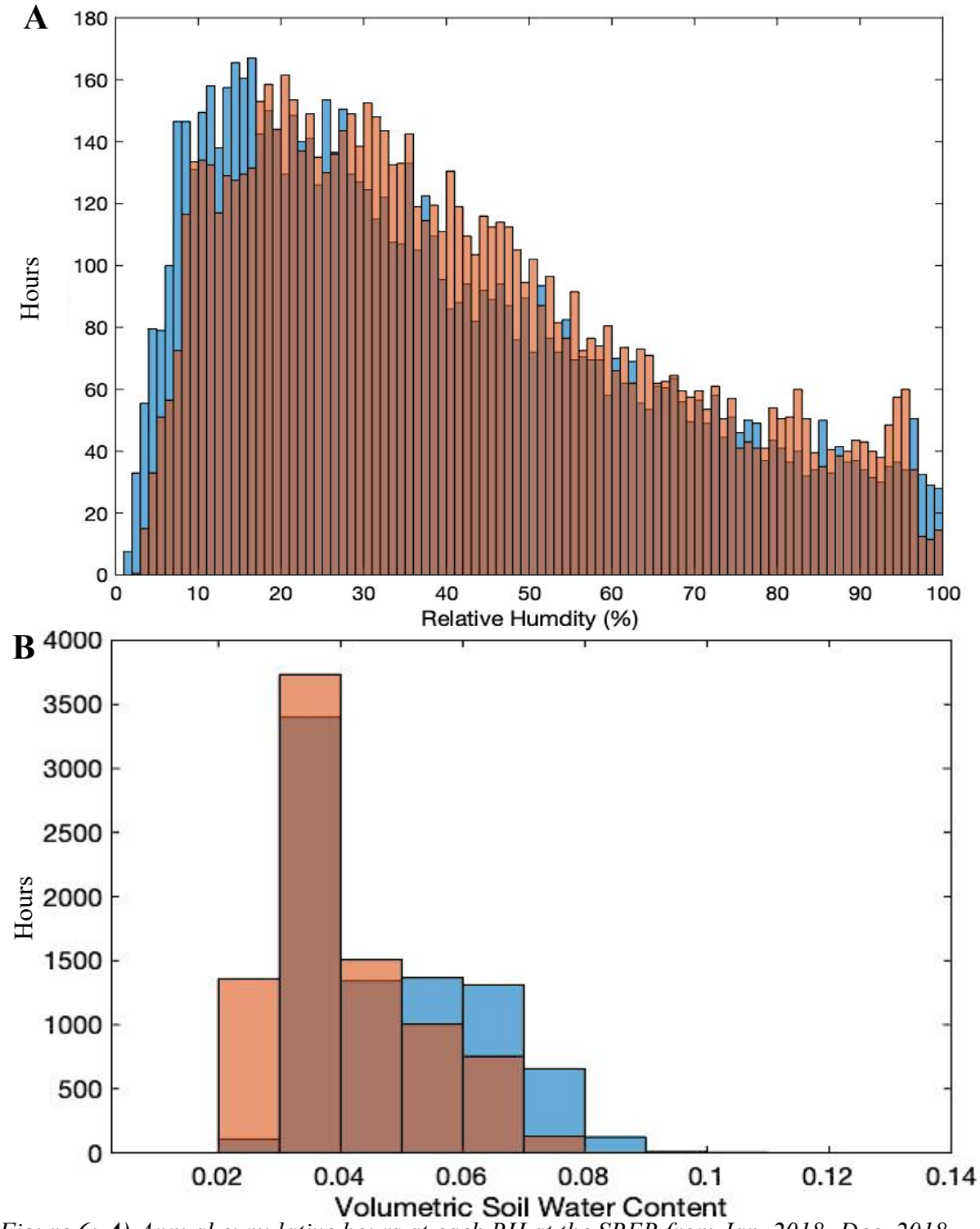

*Figure 6: **A)** Annual cumulative hours at each RH at the SRER from Jan. 2018- Dec. 2018 (blue bars) and Jan. 2019-Dec. 2019 (brown bars). **B)** Annual cumulative volumetric soil water content at the SRER from Jan. 2018- Dec. 2018 and Jan. 2019-Dec. 2019.*

To remove confounding variables introduced by rainfall, fog, and dew, on the connection between atmospheric RH, atmospheric T and VSWC, SRER data was processed to remove rainy days and fog and dew periods as described in the Chapter 2 methods. Plots of atmospheric RH and T against VSWC, did not show any clear trends (Figure 9A, B). However, linear regression models of both datasets indicated that RH had a slight positive correlation with VSWC, and T had a slight negative correlation. A linear regression model of VSWC = 0.0254 + 0.00019(RH) had a p-value of 1.56×10^{-128}.

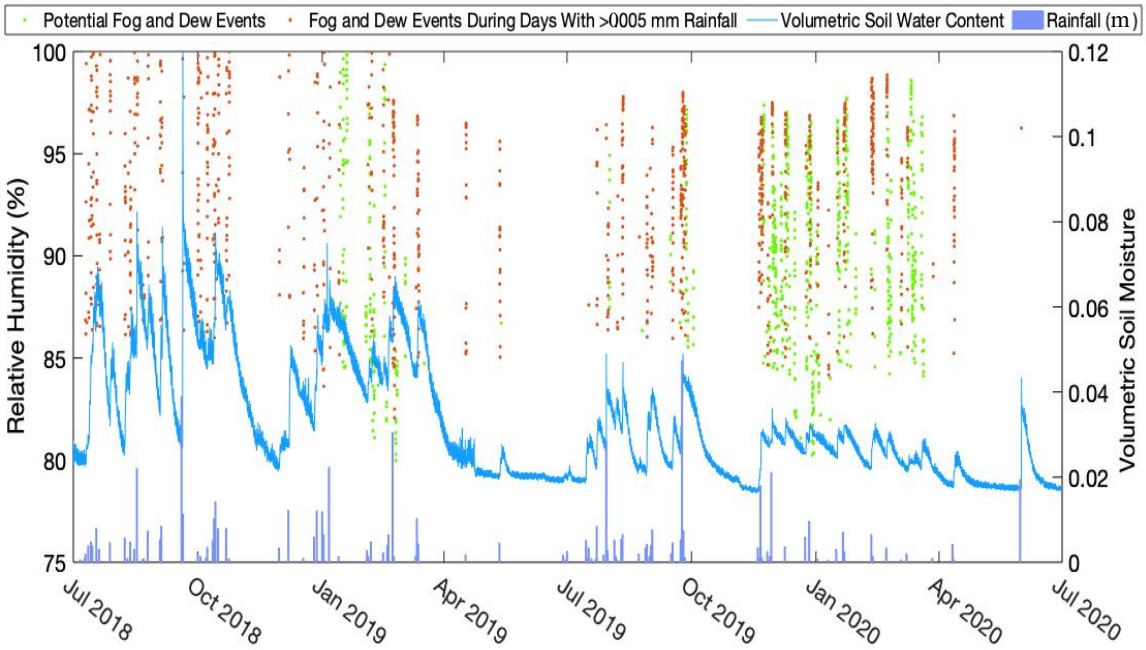

Figure 7: Left Axis: Potential fog and dew events at the SRER from Jul 2018-Jul 2020 (Green). Fog and dew events occurring during rainy days (cumulative rainfall < 0.005 mm, Red). Each Event represent a half-hour period. Potential fog and dew events were calculated to be any hourly period where average atmospheric T conditions dropped below the threshold of the dewpoint + 2.5 °C. Right Axis: Volumetric soil water content (cm^3 of water/cm^3 of soil, Blue) read at a depth of 6 cm and cumulative rainfall (m, Purple).

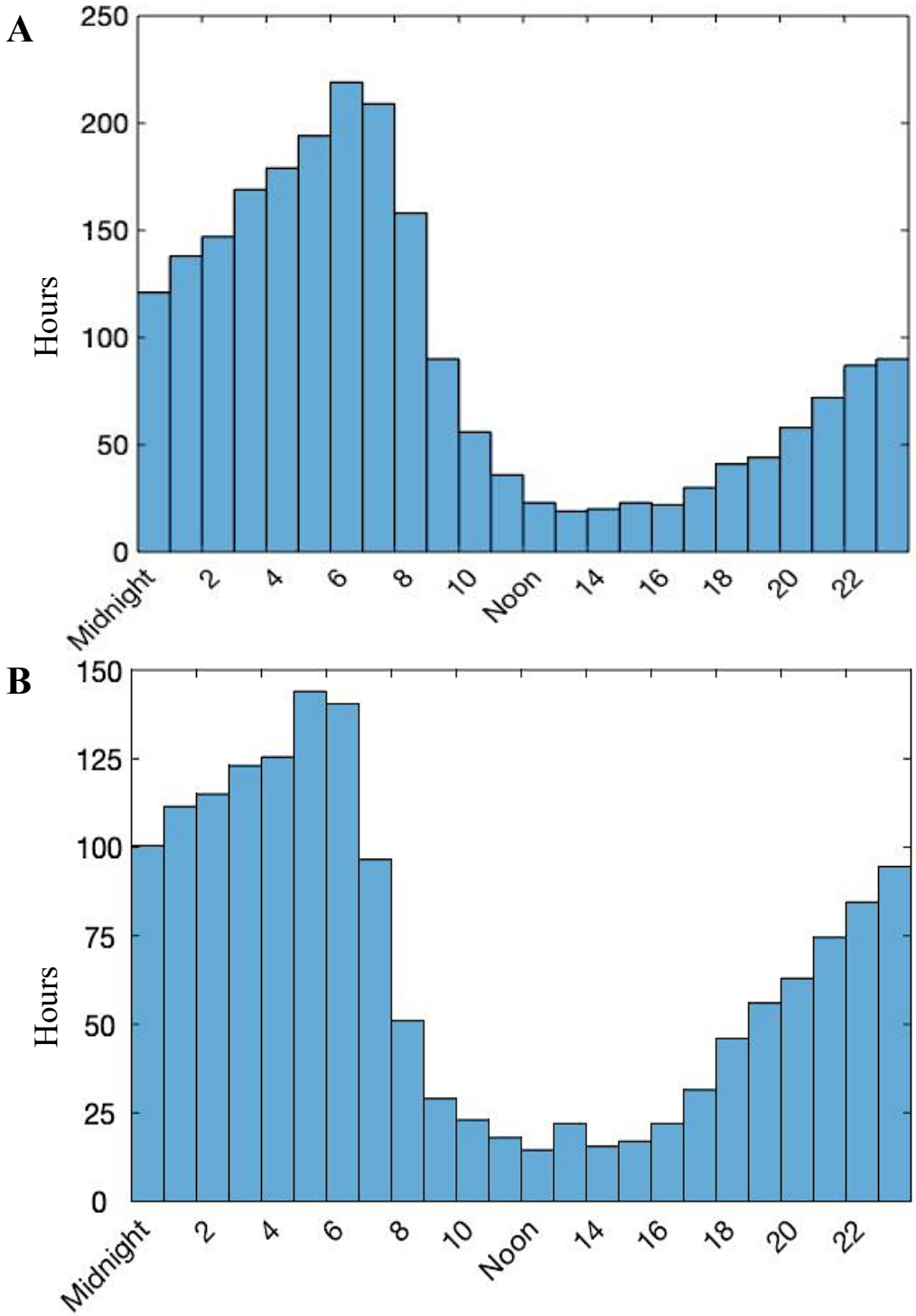

*Figure 8: Dew point data was used to estimate the diurnal cycle of potential fog and dew events at the DBG from Aug. 2016 – Dec. 2020 (**A**) and at the SRER from Jan. 2019 - Dec. 2020 (**B**). Potential fog and dew events were calculated to be any hourly period where average atmospheric temperature conditions dropped below the threshold of the dewpoint + 2.5 °C.*

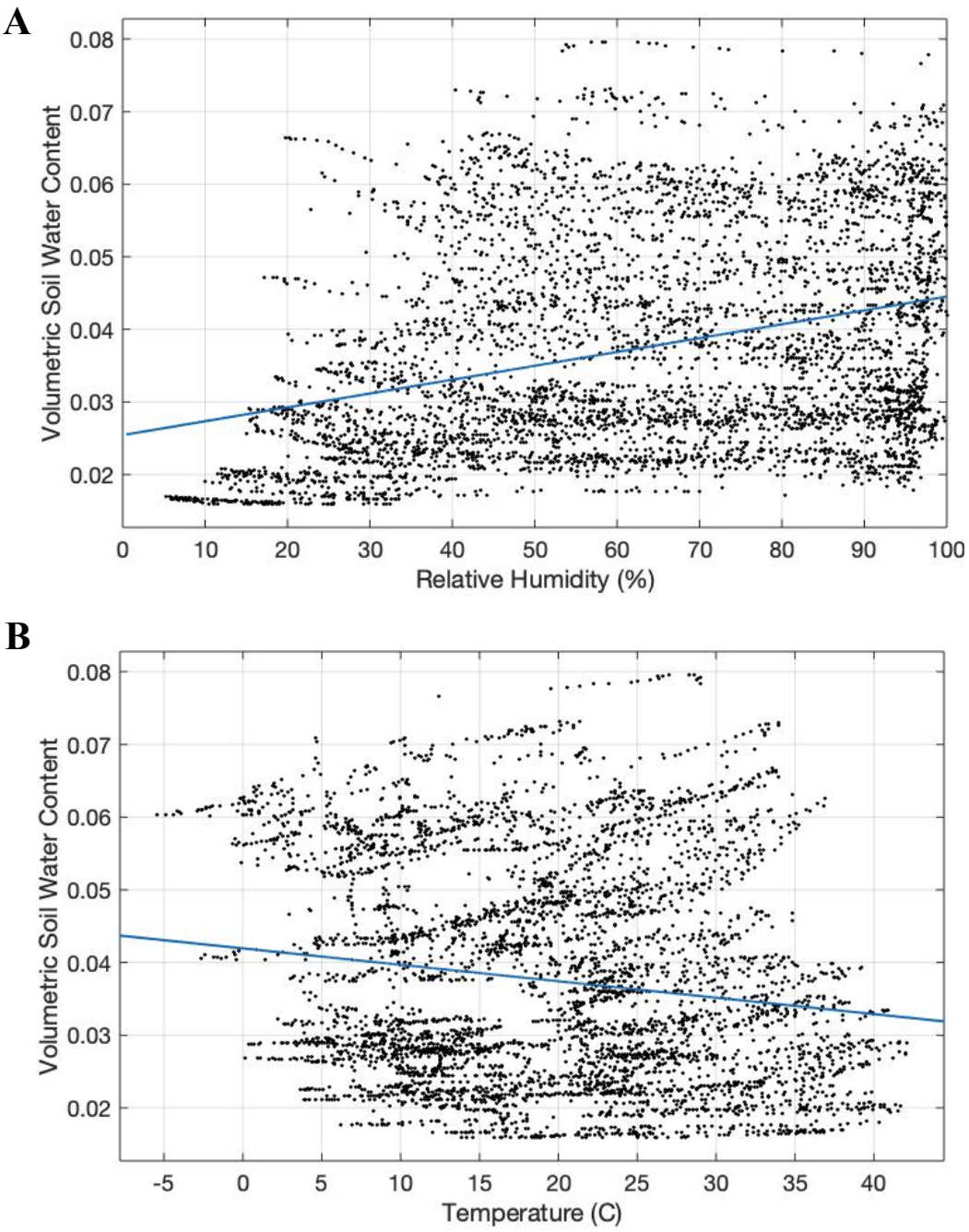

Figure 9: Data from the SRER from Jul. 2018 – Aug. 2020 were analyzed to remove periods of rainfall, and potential fog and dew. Each data point represents a 30-minute period. Volumetric Soil Water Content (VSWC) was measured using a Sentek TriSCAN EnviroSCAN soil moisture sensor inserted at a depth of 6 cm. ***A)*** *VSWC was plotted against atmospheric RH collected at a height of ~ 2m above the soil surface and the linear fit, VSWC = 0.0254 + 0.00019(RH), was plotted.* ***B)*** *VSWC was plotted against atmospheric T collected at a height of ~ 2m above the soil surface and the linear fit,*

and an R^2 value of 0.109. The low p-value indicates that there is a significant, if very small, positive correlation between RH and VSWC; however, the low R^2 value indicates that the model is insufficient to make any meaningful predictions of VSWC from RH. A similar linear regression model of VSWC = 0.0419 + -0.0002(T) had a p-value of 1.58 x 10^{-25} and an R^2 value of 0.0214, indicating a significant, but unpredictive negative correlation between T and VSWC at the SRER.

To determine if changes in VSWC are correlated with any atmospheric variables, the changes in VSWC (ΔVSWC) for each 30-minute period were compared to RH, T, and the changes in both variables over each equivalent 30-minute period (ΔRH and ΔT, respectively). Plots of ΔVSWC against RH, ΔRH, T and ΔT (Figures 10A, 10B, 11A, and 11B) showed no clear correlations between ΔVSWC and any variable. Linear regression models of each dataset were performed; however, only small, significant positive or negative correlations were found. However, the comparison of RH and ΔVSWC did demonstrate greater scatter above 75% RH and, similarly, as T lowered the scatter of T against ΔVSWC also seemed to increase in breadth.

Discussion

Historical Weather Data Analyses

Atmospheric RH and soil water content were evaluated at the SRER to determine if the frequency and duration of NRM events could be determined using historical atmospheric RH conditions. Analyses of the RH data from both sites indicated that there are hundreds of hours of elevated RH at both the DBG and

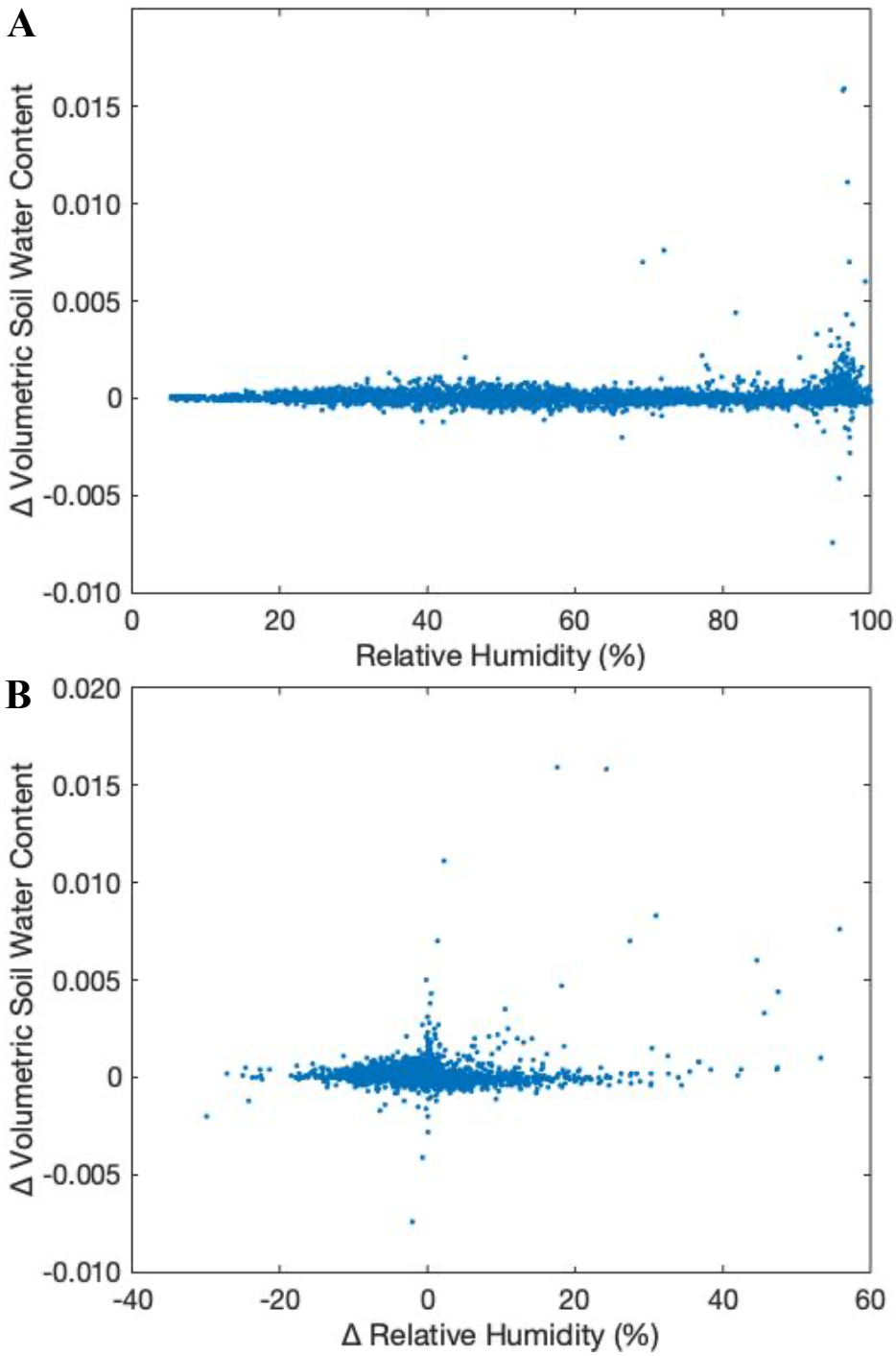

Figure 10: VSWC and RH data from Figure 9A was analyzed to determine the change in both variables across 30-minute periods. ***A)*** *ΔVSWC was plotted against atmospheric RH.* ***B)*** *ΔVSWC was plotted against ΔAtmospheric RH.*

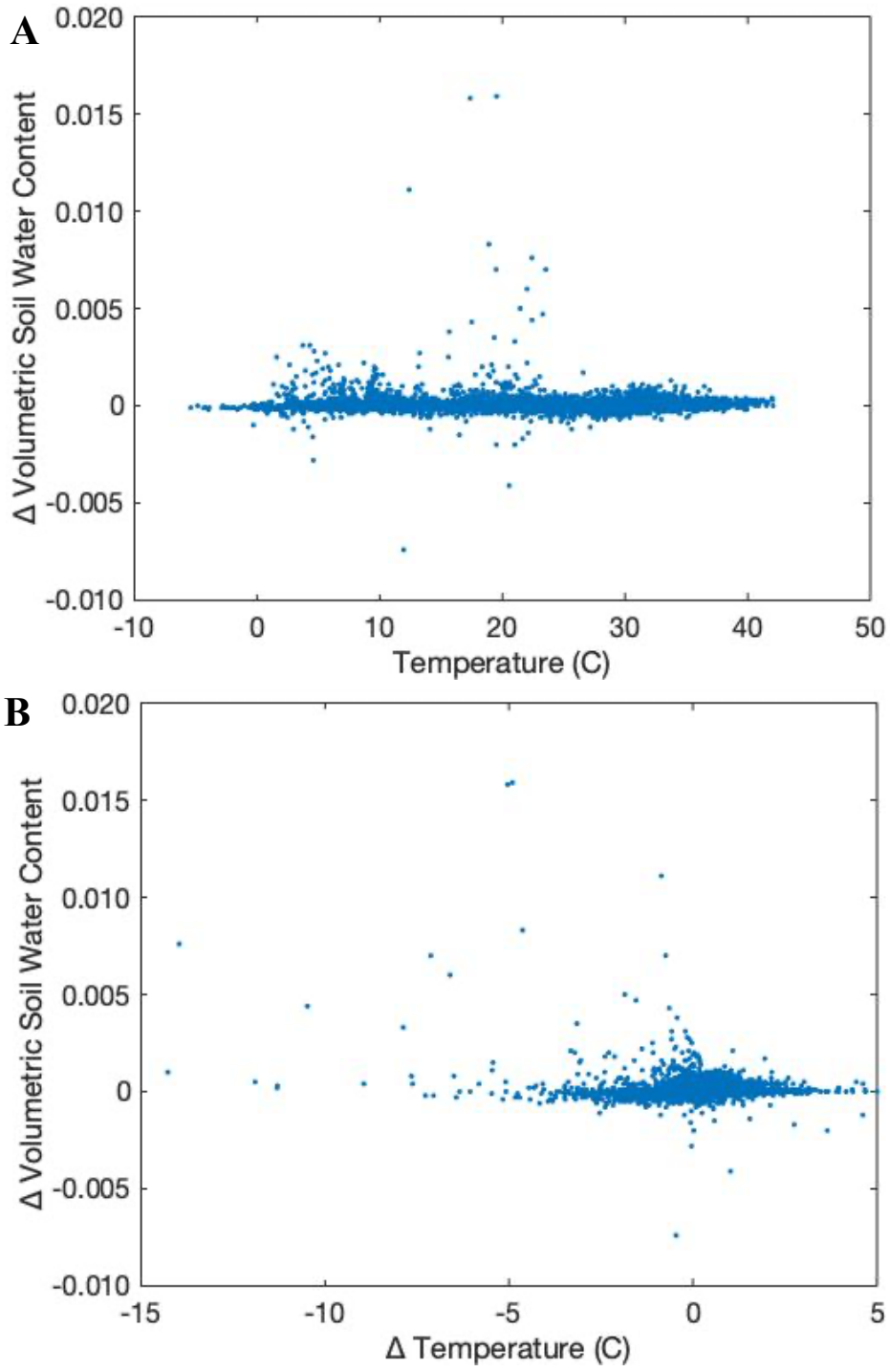

Figure 11: VSWC and atmospheric T data from Figure 9B was analyzed to determine the change in both variables across 30-minute periods. ***A)*** *ΔVSWC was plotted against atmospheric T.* ***B)*** *ΔVSWC was plotted against ΔAtmospheric T.*

SRER (Figure 5, 6). And, while both sites primarily experience lower relative humidity, there are significant quantities of time that each site spends above 75%, 85% and even 90% RH.

Overall, the lack of any significant predictive power on VSWC between either atmospheric T or atmospheric RH indicates two potential possibilites. While it is possible that soil moisture is only very slightly affected by either variable, positively by RH and negatively by T, it seems unlikely as other previous research has found direct correlations between elevated RH and NRM events. Another reason that VSWC seems unaffected by atmospheric inputs could be the depth of the soil moisture sensor. At 6 cm depths, it is likely that only very large water inputs such as rainfall will affect soil moisture readings. This is somewhat supported by the soil moisture trend (Figure 7, Appendix B Figure 21). However, some soil moisture events did occur at higher humidities as the comparisons of RH and ΔVSWC did have greater scatter above 75% RH. If these events are due to the elevated humidities, it could be indicative that only longer periods of high humidities could impact soil moisture at that 6 cm depth (Appendix C Figure 23, 24), the NEON standard. In that case, particularly in dryland regions, it may be necessary to employ more sensitive soil moisture sensors, capable of measuring smaller changes in soil moisture with less uncertainty, much closer to the surface in order to determine how and when NRM events may be occurring and to what degree these events could impact the very near surface soils.

While fog and dew conditions are far less frequent than elevated RH, NRM events could still be occurring during high RH events that do not fall to low enough T to reach the dew point. Neither soil water vapor adsorption nor deliquescence rely on T to drive

their occurrence and could therefore be occurring during these elevated RH events if soil conditions are appropriate. However, without models to demonstrate how the VSWC of the soil changes with RH, it is not possible to estimate how these other NRM sources impact the soils at these sites without soil moisture data.

Comparing the precipitation and soil moisture data at the SRER indicates that the majority of large soil moisture events (> 0.02 increase in VSWC) are likely due to rainfall. Additionally, these large soil moisture events tended to have significant lag times before returning to the typical 'dry' VSWC of the soil at the SRER which appears to be around 0.02 VSWC. However, smaller increases in VSWC occurred throughout the year and during the lag times of larger events. While some of these events may also be indicative of rainfall, others may be indicative of small fog and dew events, particularly those that occurred during the early spring when rainfall tended to be lower. Although it is possible for some NRM events to have occurred based on the soil moisture data, it is difficult to deconvolve the effects of rainfall on soil moisture. To do so, specific laboratory testing of how VSWC changes with RH for the soil at a given site is necessary.

CHAPTER 3

EARTHPOD SENSOR ARRAYS

Introduction

While remote sensing can provide insights into even relatively small phenomena like vegetative cover, it excels at providing data and readings at broader spatial scales. Local measurement systems can gather data on much finer scales, but are less suited to gathering broader, regional measurements (Bogena *et al.*, 2007). Proximal soil property sensing is particularly valuable to understanding the specific characteristics of heterogenous microclimates and ecosystems such as those found in drylands, but is not enough to deeply characterize the environmental dynamics of these regions (Rossel *et al*., 2011). Environmental Sensor Networks (ESNs) may provide a solution. ESNs use arrays of sensor nodes that can provide measurements of more variables on significantly finer spatial and temporal scales than remote sensing and bridge the gap between local environmental variables and their distribution over broad areas (Zerger *et al*., 2010; Bogena *et al.*, 2007). ESNs have the added benefit of providing and storing data in real-time. Besides providing situational awareness, live-streaming and hosting data over the internet provides the distinct advantage of being able to readily respond to events of interest or even, as sensor networks develop, remotely modify measurement techniques and methods to better respond to real-time events (Liang *et al.*, 2005; Zerger *et al.*, 2010; Bogena *et al.*, 2007).

In drylands, where environmental variables can vary between microclimates on submeter scales and can change based on broader climate or ecological factors on the scale of hundreds of hectares, ESNs are essential to any deep understanding of regional

soil dynamics (Browning *et al.*, 2015). Previous work applying ESNs to dryland regions has primarily focused on agricultural applications. ESNs measuring soil water dynamics over large areas on fine scales have successfully been applied to agricultural field sites in the northwestern U.S. (Gasch *et al*., 2017). Outside of agricultural work, ESNs applied to dryland regions still typically focus on characterizing water dynamics, particularly water pulses, to better understand vegetative growth, desertification, and erosion in North American desert regions (Collins *et al*., 2014; Browning *et al*., 2015). ESNs with a specific focus on measuring environmental variables of relevance to microbial growth and activity are an essential link between local microbial studies and cross-scale analyses of regional and global dryland microbial elemental cycling.

To that end, an ESN, with nodes termed EarthPods, focused on atmospheric RH, pressure, and T was designed for use in very near surface (< 6 cm) measurements. These EarthPods were also equipped with two invasive sensors to measure soil moisture, T, and RH. This chapter focuses on the design and testing of these EarthPods and provides recommendations for sampling schemes in the future.

Computing

The primary computing device used in the construction of the EarthPods was the Adafruit Feather M0 WIFI. This board uses an ATSAMD21G18 ARM Cortex M0 microcontroller, which is fully compatible with the Arduino IDE used to program each pod. The M0 is also equipped with an ATWINC1500 network controller, capable of streaming data packets over a WiFi network.

The Feather is attached to a larger board equipped with a variety of other essential capabilities and interfaces for sensors and data storage. Each board is equipped with an Adafruit SDIO MicroSD Card reader for backup data storage and dedicated SPI and I^2C buses for interfacing with external sensors. In particular, the I^2C bus is easily accessible at the top of the board and can be used for a far larger variety of sensors than were equipped to the EarthPods here.

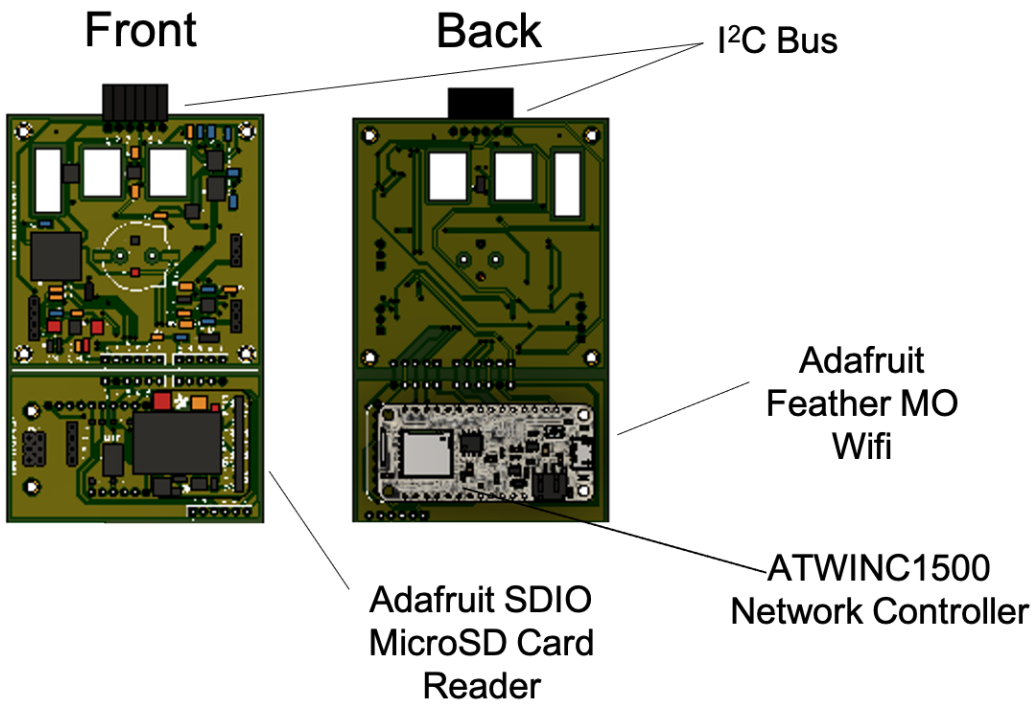

Figure 12: Schematic of EarthPod Boards Designed by Cole Baurer and Katrina Davis

Packaging

The EarthPod packaging was designed to both protect the boards from inclement weather and allow sufficient airflow for internal, protected atmospheric sensors.

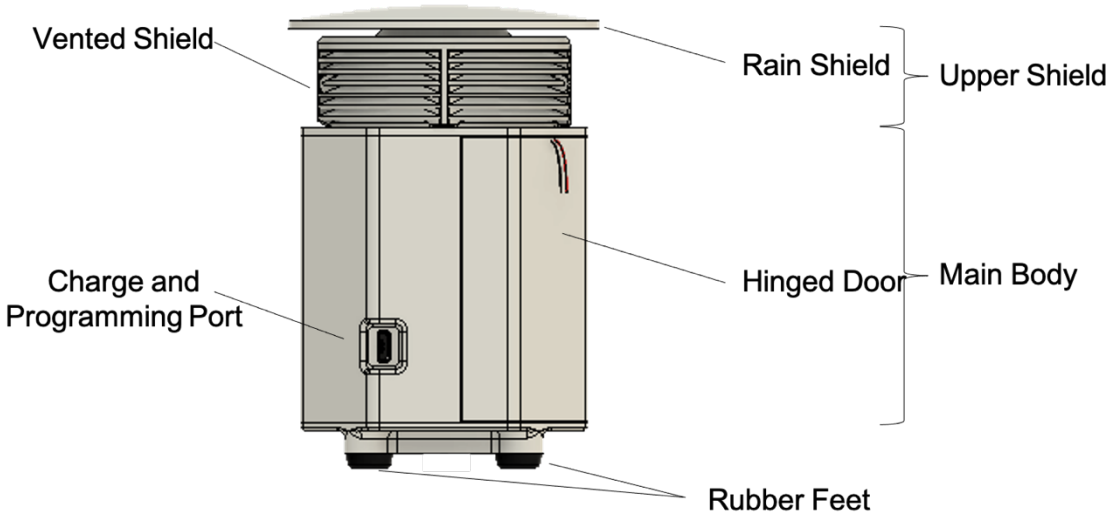

Figure 13: Schematic of EarthPod Casing Designed by Cole Baurer

The upper shield of the EarthPod casing was designed to address these potential issues. The rain shield protects sensitive electronics from rain and high T and the vented shield allows airflow into and out of the inner chamber of the EarthPod, allowing cooling and atmospheric equilibration for sensors. The main body of the casing was designed to both protect the boards and allow easy access for charging, programming, and repair. In addition, the whole casing is elevated by 1 cm on four rubber feet to avoid low-level running water and maintain stability.

Sensors

Internally, the EarthPods were equipped with both and Si7021-A20 I^2C atmospheric RH and T sensor and an SPL06-007 pressure and T sensor. The Si7021-A20

sensor can take readings of RH between 0-80% to at least 3% accuracy and T between -10 to 80°C to at least 0.4°C accuracy. Similarly, the SPL06-007 sensor can report pressures of 300-1100 hPa to 1 hPa accuracy and T of -40 to 85°C to at least 0.5°C accuracy.

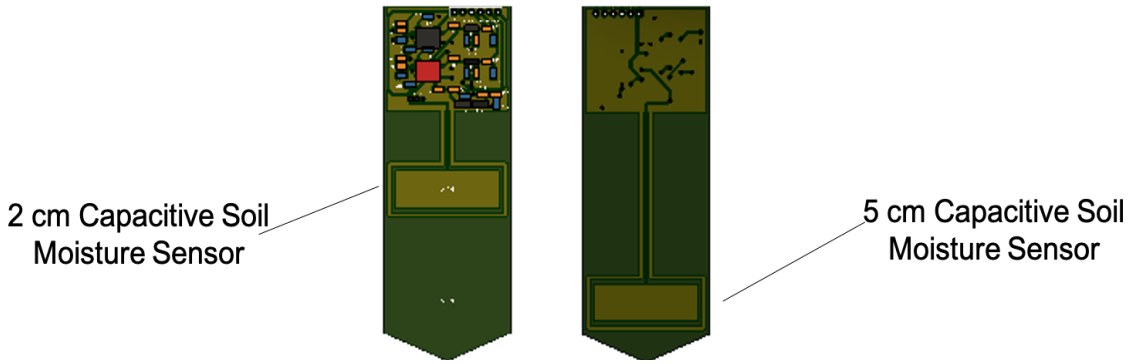

Figure 14: Schematic of Capacitive Soil Sensor Designed by Katrina Davis

Two external sensors were attached to the EarthPods. The Adafruit AM2315 Encased Atmospheric Temperature and Humidity sensor and a new capacitive soil moisture sensor designed by Katrina Davis. Both sensors use capacitive measurement systems to determine the RH of the air or soil moisture, respectively. The AM2315 is capable of measuring RH of 0-100% to at least 3% accuracy and T of -20 to 80°C to at least 0.3°C.

The newly designed soil moisture sensor (Figure 14), uses a voltage divider to measure the capacitance of the surrounding soil at two depths, 2 cm and 5 cm. This system of measurement works using the soil as one of two resistors that make up the voltage divider. As the water content of the soil increases, so too does the dielectric constant of the soil. As the dielectric constant increases the voltage output through the voltage divider decreases, resulting in a reading reflecting an inverse relationship between moisture and voltage. The dielectric constant of soil is, however, extremely

variable. Various other soil characteristics, including soil texture and porosity, mineral content, and T, can all impact these readings. It is therefore necessary to calibrate these sensors to site-specific soils prior to deploying in field environments.

Laboratory Manipulation Methods

The AM2315 was tested to determine its ability to assess soil moisture during a soil core dry down experiment. A soil core was collected and the AM2315 was inserted to a depth of 1-3 cm. The 800g core was wetted using ~18 g of water, until the surface of the core visually appeared near or at saturation. The soil core was then allowed to dry over the course of 5 days at room T (20 – 24°C) and soil RH and T were taken every 3 minutes. These tests indicated that the AM2315 was fully capable of seeing small and rapid changes in soil RH (Figure 15).

Humidity chambers were composed of sterilized Coleman 48-quart performance coolers. Saturated salt solutions maintained a constant RH in the headspace of the humidity chamber ($MgNO_3$ 53%, NaCl 76%, and K_2SO_4 98% RH at 10°C; Rockland, 1960). Soil samples were collected and dried overnight at 105°C. EarthPod soil moisture and RH probes were inserted at a depth of 2 cm and 0-2 cm into the dried soil, respectively. Over a 3-day period from Oct. 9th-11th, the soil sample was placed in each of the three humidity chambers for at least 12 h each in order from lowest to highest humidity. In between each humidity chamber, soil samples were dried overnight at 60°C. From Oct. 13th-15th this process was repeated with the 53% and 98% humidity chambers. During the first 60°C drying process, overnight from Oct. 9th-10th, the EarthPods and their sensor were kept inserted. Atmospheric RH and T and soil moisture data was

collected during each humidity manipulation and during the first drying step. Soil RH and T data was not collected until Oct. 13th-15th due to battery issues.

Data collected from each EarthPod was streamed to a dedicated DeepGIS sensor page, http://sensors.deepgis.org:4000/. Data was processed in MATLAB. Linear regression models were performed using the fitlm function and first order polynomial curves were fit using the MATLAB Curve Fitting App.

Sampling and Calibration

Prior to deploying the EarthPods, the AM2315 was tested for its ability to assess soil RH. The resulting data indicated that while soil RH began increasing immediately following the wetting event, the drying of the soil core is mimicked closely by the soil RH measured by the AM2315. There is some lag time post-wetting, prior to the maximum RH reading; however, this is likely due to the time it takes for water vapor from the wetting event to move down to the active sensing region from 1 – 3 cm depths.

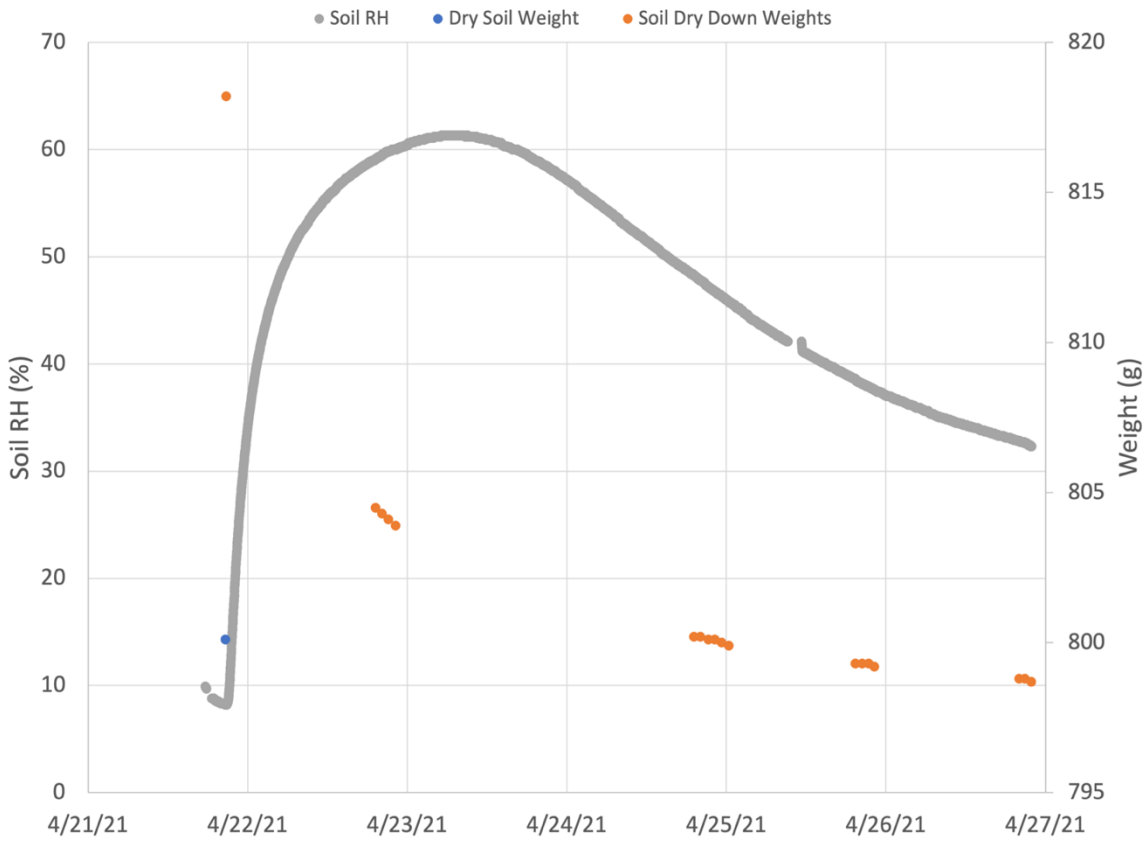

Figure 15: Test of the Ability of the AM2315 to assess Soil RH. The sensor was inserted from 1-3 cm depth and water was added to a soil core until the surface was at or near saturation. Cores were dried at room temperature over the course of a 5-day period. Soil RH (gray) was collected every 3 minutes. Core weight (initial-blue, dry down-orange) was collected using a Mettler Toledo M13001t scale.

EarthPods were deployed in soil for testing. While the casing was placed directly on the soil surface (elevated by the rubber feet by ~ 1 cm) giving atmospheric T and RH readings at ~ 5 cm above the soil surface, the AM2315 sensor was deployed directly into the soil, reading the RH and T over a range of approximately 0-2 cm below the soil's surface. The novel soil moisture probe was inserted such that each strip read the capacitance of the soil at 2 and 5 cm respectively. The AM2315 and the novel soil moisture probe were both inserted and stabilized in the soil with a brief wetting event. Data was streamed to ThingSpeak using the ThingSpeak Arduino library.

Data collected over the course of 3 days of deployment indicated that surface soil T and atmospheric T were very tightly correlated and that, although the soil RH started in a higher range due to the insertion procedure, it quickly equilibrated to a diurnal cycle reaching a maximum around the same maximum RH as the atmospheric RH and a minimum ~ 20% above the minimum atmospheric RH (Figure 16).

Using soil from the same location, it was also possible to calibrate the novel soil moisture sensor to make a model estimating the gravimetric water content of the soil (Figure 17). Soil was dried overnight at 105°C. The dried soil was then weighed (90 g) and water was added stepwise (4.5 g or 5% of total soil weight) until the soil reached saturation. A first order polynomial function, $f(x) = -0.07459x + 1059$, was fit to the data using the MATLAB Curve Fitting Tool. The R-Square value of 0.9939 and the RMSE of 0.006527 indicate that the calibration curve could give an accurate estimation of soil gravimetric water content between 0 and 0.2, completely dry and saturated respectively.

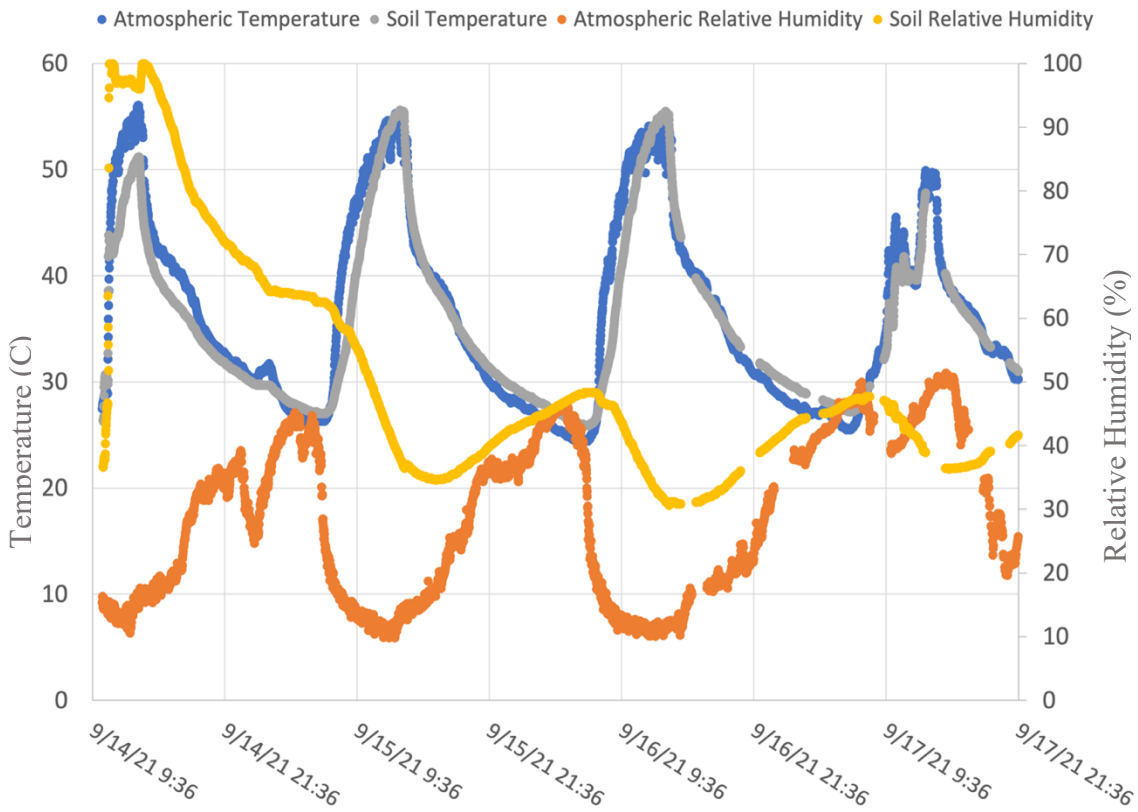

Figure 16: During the first outdoor EarthPod installation and test, data was collected between 9/14 and 9/17. Atmospheric T and RH (Blue and Orange, respectively) were collected inside the EarthPod housing and Soil T, and Soil RH (Gray and Yellow, respectively) were collected by the AM2315 sensor inserted from 0-2 cm depth.

To determine if sustained periods of elevated RH could directly impact gravimetric soil water content (GSWC, g of water/g of soil), soil samples were placed progressively in three humidity chambers with increasing RH as described in the methods section. EarthPod sensor arrays were placed in the humidity chambers and soil samples to

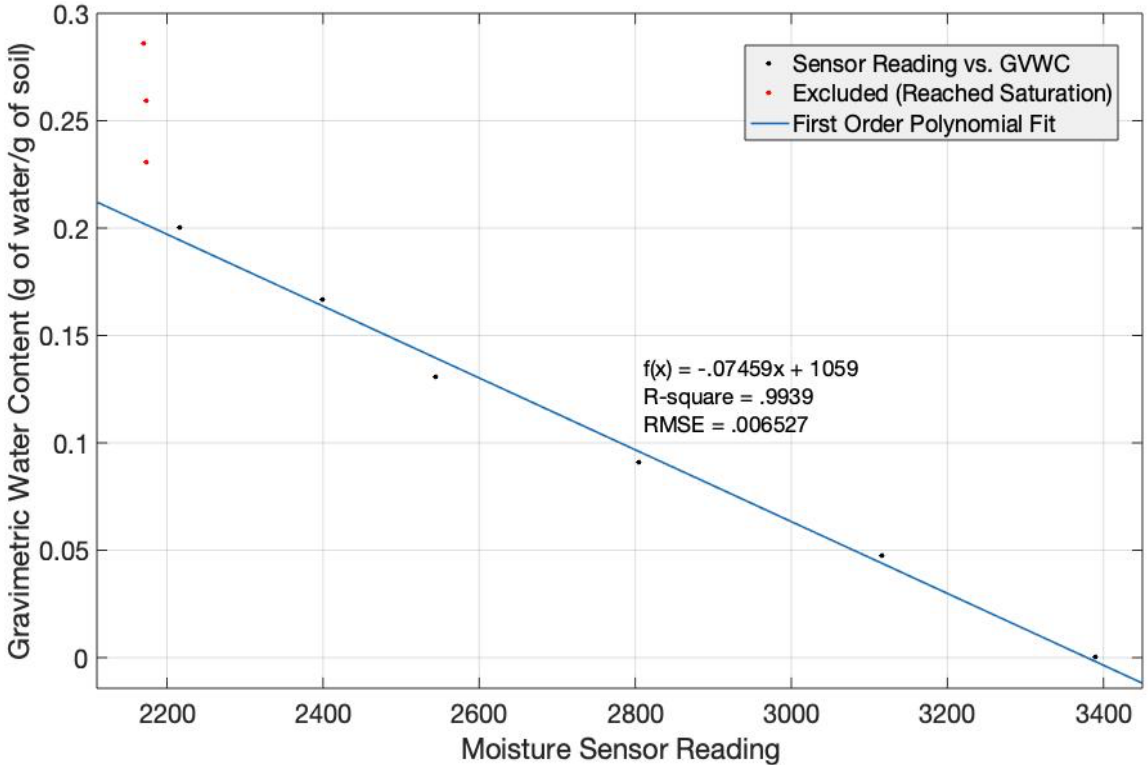

Figure 17: Calibration curve of novel moisture sensor reading against gravimetric water content. Each point, from right to left, represents approximately a 5% by soil weight addition of water. A first order polynomial fit was found using the MATLAB Curve fitting tool.

monitor both atmospheric and soil variables. Plots of GSWC and atmospheric RH (Figure 18, A) show a positive correlation between the experienced atmospheric RH and the GSWC. A linear regression model of this data set indicates that a model of GSWC = -0.0165 + 0.0004 Atmospheric RH) with a P-value of 0 and an R^2 value of 0.736. This also supports that atmospheric RH has a positive correlation with GSWC, but that the model has insufficient predictive power. From this initial analysis of the soil RH measurements compared to the GSWC, we observe the soil RH, which remains at or very

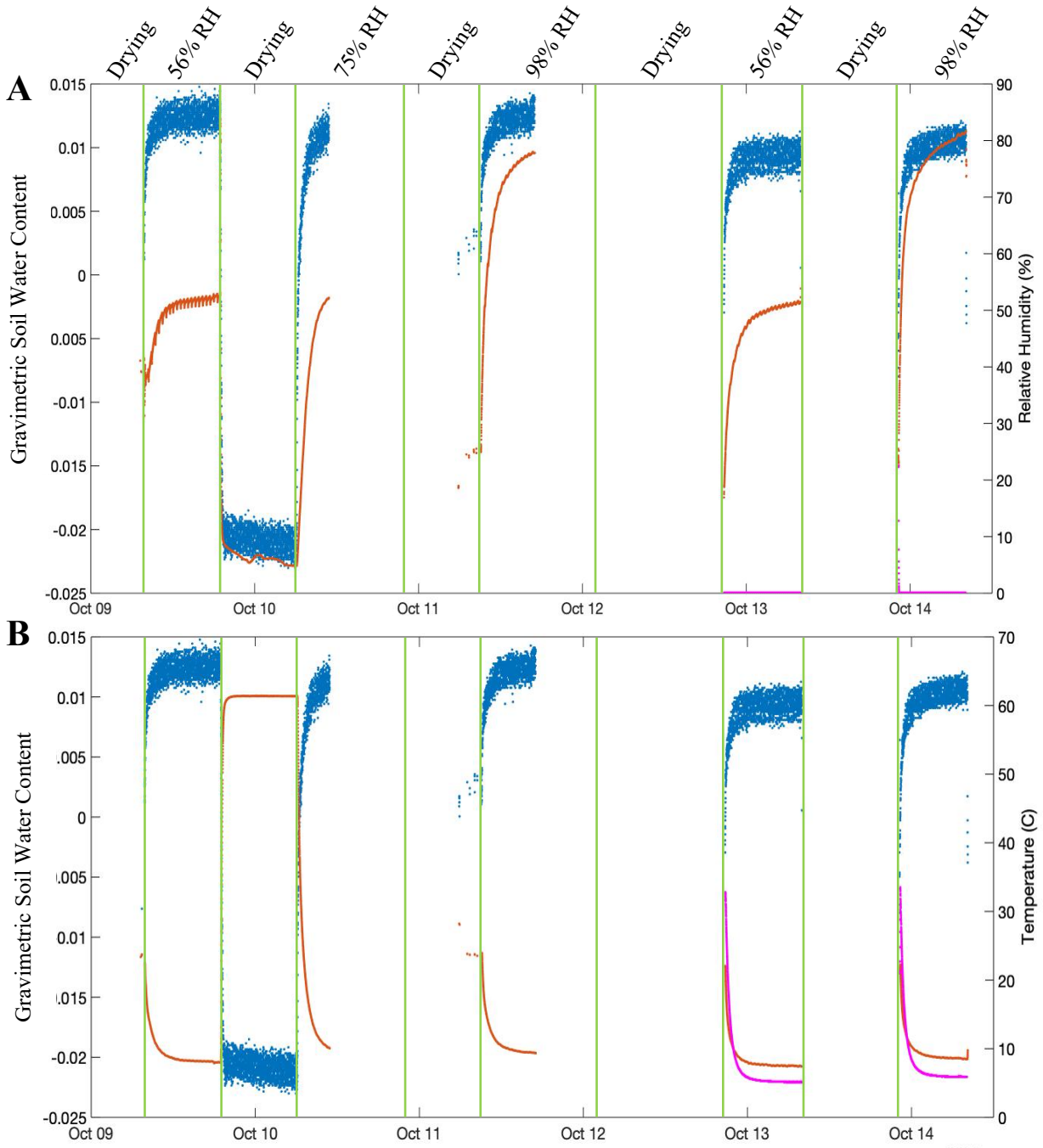

Figure 18: Gravimetric Soil Water Content, RH and T data were collected with EarthPod sensor arrays in humidity chambers at 56%, 75%, and 98% RH. GSWC was calculated using the linear fit model described in chapter 3. ***A)*** *GSWC (Blue, left axis), Atmospheric RH (Orange, right axis), and Soil RH (Magenta, right axis).* ***B)*** *GSWC (Blue, left axis), Atmospheric T (Orange, right axis), and Soil T (Magenta, right axis).*

near 0 from Oct. 13th- 15th is not predictive in the change in the GSWC readings provided by the novel soil moisture sensor.

An analysis of the atmospheric T against measured GSWC (Figure 18, B), indicates that there is a strong negative correlation between the GSWC readings by the novel soil moisture sensor and the atmospheric T. A linear regression model of these variables indicates that a model of GSWC = 0.016388 + -0.00059983 (Atmospheric RH) with a p-value of 0 and an R^2 value of 0.975. As opposed to previous models, this indicates both a significant negative correlation between atmospheric T and measured GSWC and that the linear regression model of atmospheric T has some degree of predictive power for GSWC. A linear polynomial fit was made to compare these two variables (Figure 19, A), this model indicated that of the observed data points the model closely fit within error as demonstrated by an RMSE of 0.0020.

A similar analysis was performed to compare soil T and GSWC (Figure 19, B from Oct.13th -15th). Plots of these variables indicated a similar but more consistent negative correlation as with atmospheric T. Similarly, fitting a linear regression (Figure 19, B) indicated a fit of GSWC = -0.0003154(Soil T) + 0.01478.

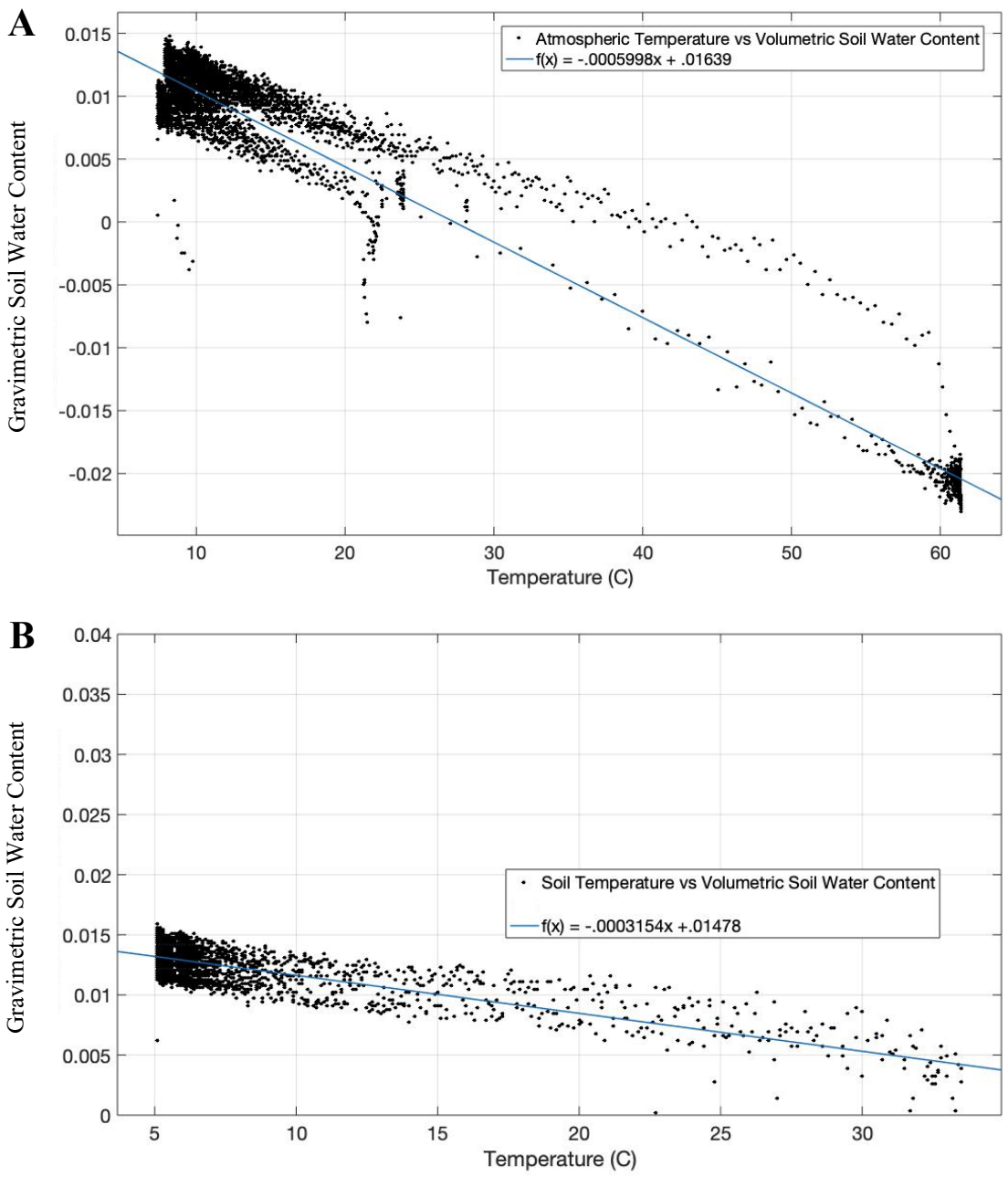

Figure 19: Gravimetric soil water content (GSWC) was calculated using the calibration curve in Figure 17. GSWC and T data from Figure 18 were analyzed using the MATLAB Curve Fitting App to fit first order polynomial curves. ***A)*** *GSWC was plotted against atmospheric T data. The function f(x) = -0.0005996x + 0.01639 fit the data with an* R^2 *value of 0.9751 and an RMSE value of 0.001998.* **B)** *GSWC was plotted against soil T data. The function f(x) = -0.0003154x + 0.01478 fit the data with an* R^2 *value of 0.5465 and an RMSE value of 0.001338.*

Discussion:

The data collected in the humidity chamber manipulations implied some small correlation between increased RH and GSWC. However, since the change in GSWC appears to be approximately the same during each event while RH changes significantly, it is likely that some other factor is driving the change in GSWC reading. Similarly, since the soil RH does not seem to change during these humidity events, it may be possible that there is no actual change in soil moisture and that some other variable is affecting the measured value of the capacitive soil moisture sensor. It is also possible that the depth of both the soil moisture sensor and the RH sensor (2 cm), although closer to the surface than the sensors array at the SRER, still precludes any sensing of very surficial NRM soil moisture events.

However, the T data seems to provide an answer to these questions. While the humidity chamber manipulations suggests a strong, predictive correlation between soil moisture and atmospheric T, it is more likely that the capacitive soil moisture sensor readings are affected by changes in T. The soil moisture sensor functions by measuring the dielectric constant of the soil and, while this constant is strongly impacted by soil moisture, it is also sensitive to other variables including T. In particular, the large negative change in GSWC during the drying step from Oct. 9^{th}-10^{th} (Figure 18 B), which brought the GSWC down to a below 0 reading, indicates that T is also impacting the soil dielectric constant of the soil confounding the actual value. It is therefore important to further test and develop the novel soil moisture sensor to determine what specific T effects have on soils and calibrate the sensors such that changes in T do not obscure actual soil moisture readings. Fortunately, the strong, significant correlations found here

using the linear regression of T and gravimetric water content can be used to calibrate the soil moisture sensors for future research with some changes as new sensors are developed. In particular, these sensors have have the potential to charecterize small, surface soil water inputs that may directly impact microbial activity in these regions. Further development and testing is needed; however, this work lays the foundation for microbial studies that correlate dryland microclimates with specific, correlated microbial activities on the genetic and transcriptomic level.

CHAPTER 4

CONCLUSIONS

While rainfall proved to be the largest factor in increasing soil moisture (Figure 7), especially for large increases in water content, > 0.02 VSWC, NRM events are not precluded from impacting dryland soils. Particularly for surficial soil (0-2 cm), potential fog and dew events may occur with enough frequency beyond rainfall events that they impact microbial metabolisms and elemental cycling that occurs in dryland soils (Figure 7). While both sites spent significant quantities of time at elevated RH, surprisingly, only small correlations were found between atmospheric RH and soil water content. This is opposed to previous research performed on NRM moisture, which demonstrated significant correlations between increasing RH and surface litter moisture events as measured by leaf wetness sensors (Evans *et al*., 2020). While these correlations were statistically significant, the models proved insufficient to predict when a soil moisture event could occur based solely on RH data. To some extent, these results could be expected. A potential explanation for these results could be the uncertainty in the soil water content. The SRER data reported a minimum uncertainty of around 7% water content, which for the extremely small changes in soil moisture that could be expected from NRM events, could easily obscure any significant changes in water content that occurred due to RH. However, the more likely explanation for the lack of connection between these two variables is that the only soil moisture data available from the SRER was read at a minimum depth of 6 cm, which could simply be too deep for the atmospheric variables to have any clear impact on soil conditions (Appendix C Figure 24). It is therefore important to further test and develop novel soil moisture sensors with

greater sensitivities and to emplace ESNs with moisture sensors at much shallower depths to catch the small changes in the very surface soils.

While the EarthPod ESN is a step in this direction it is important to determine what specific T effects have on soil moisture readings for the novel moisture probe. Using the linear regression found in Figure 19B, it should be possible to calibrate the sensors such that changes in T do not obscure actual soil moisture readings.

Future work in drylands will benefit greatly from the greater understanding of NRM and environmental variables that ESN networks like EarthPods provide. In particular, microbial studies require a deeper understanding of the environments that they are performed in. Despite the profound importance dryland microbial systems have for global cycling of CNS, dryland regions are critically under sampled for gene-based analyses. As of April 2021, the 16,462 terrestrial samples in the JGI Genomes Online Database (GOLD https://gold.jgi.doe.gov/), only 430 biosamples were taken from drylands, representing only ~2% of the total catalog. The impact of NRM moisture on these systems is also under sampled. However, without a deeper understanding of how these NRM events occur, novel gene-based studies will not be able to determine the impact NRM moisture may have on global elemental cycling.

REFERENCES

Agam, N. and Berliner, P.R. (2006) Dew formation and water vapor adsorption in semi-arid environments—A review. *Journal of Arid Environments* **65**: 572–590.

Ahlström, A., Raupach, M.R., Schurgers, G., Smith, B., Arneth, A., Jung, M., et al. (2015) The dominant role of semi-arid ecosystems in the trend and variability of the land CO2 sink. *Science* **348**: 895–899.

American Meteorological Society, (2020) Fog. Glossary of Meteorology, http://glossary.ametsoc.org/wiki/climatology.

Austin, Amy T., et al. "Water Pulses and Biogeochemical Cycles in Arid and Semiarid Ecosystems." Oecologia, vol. 141, no. 2, Springer-Verlag, 2004, pp. 221–35, doi:10.1007/s00442-004-1519-1.

Bogena, H., et al. "Evaluation of a Low-Cost Soil Water Content Sensor for Wireless Network Applications." *Journal of Hydrology (Amsterdam)*, vol. 344, no. 1, Elsevier B.V, 2007, pp. 32–42, doi: 10.1016/j.jhydrol.2007.06.032

Bonnail, E. et al. "Trapping Fresh Sea Breeze in Desert? Health Status of Camanchaca, Atacama's Fog." *Environmental Science and Pollution Research International*, vol. 25, no. 18, Springer Berlin Heidelberg, 2018, pp. 18204–12, https://doi.org/10.1007/s11356-018-2278-6.

Browning, Dawn M., et al. "Emerging Technological and Cultural Shifts Advancing Drylands Research and Management." *Frontiers in Ecology and the Environment*, vol. 13, no. 1, Ecological Society of America, 2015, pp. 52–60, doi:10.1890/140161.

Bünemann, E.K. and Condron, L.M. (2007) Phosphorus and Sulphur Cycling in Terrestrial Ecosystems. In *Nutrient Cycling in Terrestrial Ecosystems*. Soil Biology. Marschner, P. and Rengel, Z. (eds). Berlin, Heidelberg: Springer, pp. 65–92.

Cable, Jessica M., et al. "Soil Texture Drives Responses of Soil Respiration to Precipitation Pulses in the Sonoran Desert: Implications for Climate Change." *Ecosystems (New York)*, vol. 11, no. 6, Springer Science+Business Media, 2008, pp. 961–79, doi:10.1007/s10021-008-9172-x.

Canarini, Alberto, et al. "Quantifying Microbial Growth and Carbon Use Efficiency in Dry Soil Environments via 18O Water Vapor Equilibration." *Global Change Biology*, vol. 26, no. 9, Blackwell Publishing Ltd, 2020, pp. 5333–41, doi:10.1111/gcb.15168.

Chen, H., Liu, J., Li, D., Xiao, K., and Wang, K. (2019) Controls on soil arylsulfatase activity at a regional scale. *European Journal of Soil Biology* **90**: 9–14.

Collins, S.., et al. "A Multiscale, Hierarchical Model of Pulse Dynamics in Arid-Land Ecosystems." *Annual Review of Ecology, Evolution, and Systematics*, vol. 45, no. 1, Annual Reviews, 2014, pp. 397–419, doi:10.1146/annurev-ecolsys-120213-091650.

Davila, Alfonso F., et al. "Salt Deliquescence Drives Photosynthesis in the Hyperarid Atacama Desert." *Environmental Microbiology Reports*, vol. 5, no. 4, Blackwell Publishing Ltd, 2013, pp. 583–87, doi:10.1111/1758-2229.12050.

Dirks, Inga, et al. "Atmospheric Water Vapor as Driver of Litter Decomposition in Mediterranean Shrubland and Grassland During Rainless Seasons." *Global Change Biology*, (2009), vol. 16, no. 10, pp. 2799–812, doi:10.1111/j.1365-2486.2010.02172.

Evans, S., Todd-Brown, K.E.O., Jacobson, K., and Jacobson, P. (2020) Non-rainfall Moisture: A Key Driver of Microbial Respiration from Standing Litter in Arid, Semiarid, and Mesic Grasslands. *Ecosystems*.

Gasch, C., et al. "A Field-Scale Sensor Network Data Set for Monitoring and Modeling the Spatial and Temporal Variation of Soil Water Content in a Dryland Agricultural Field." *Water Resources Research*, vol. 53, no. 12, American Geophysical Union, 2017, pp. 10878–87, doi:10.1002/2017WR021307.

Gliksman, D., Rey, A., Seligmann, R., Dumbur, R., Sperling, O., Navon, Y., et al. (2017) Biotic degradation at night, abiotic degradation at day: positive feedbacks on litter decomposition in drylands. *Global Change Biology* **23**: 1564–1574.

Goodman, Jindra. "The Collection of Fog Drip." *Water Resources Research*, Goodman, J. (1985), The Collection of Fog Drip, Water Resour. Res., 21(3), 392-394, doi:10.1029/WR021i003p00392., vol. 21, no. 3, Blackwell Publishing Ltd, 1985, pp. 392–94, doi:10.1029/WR021i003p00392.

Jacobs, Adrie F., et al. "Dew Deposition and Drying in a Desert System: a Simple Simulation Model." *Journal of Arid Environments*, vol. 42, no. 3, Elsevier Ltd, 1999, pp. 211–22, doi:10.1006/jare.1999.0523.

Jacobson, K., Diepeningen, A. van, Evans, S., Fritts, R., Gemmel, P., Marsho, C., et al. (2015) Non-Rainfall Moisture Activates Fungal Decomposition of Surface Litter in the Namib Sand Sea. *PLOS ONE* **10**: e0126977.

Kobayashi, T., He, W., and Nagai, H. (1998) Mechanisms of evaporation from soil with a dry surface. *Hydrological Processes* **12**: 2185–2191.

Kuehn, K.A., Steiner, D., and Gessner, M.O. (2004) Diel Mineralization Patterns of Standing-Dead Plant Litter: Implications for CO2 Flux from Wetlands. *Ecology* **85**: 2504–2518.

Luo, W., Dijkstra, F.A., Bai, E., Feng, J., Lü, X.-T., Wang, C., et al. (2016) A threshold reveals decoupled relationship of sulfur with carbon and nitrogen in soils across arid and semi-arid grasslands in northern China. *Biogeochemistry* **127**: 141–153.

Manzoni, S., Schimel, J.P., and Porporato, A. (2012) Responses of soil microbial communities to water stress: results from a meta-analysis. *Ecology* **93**: 930–938.

McAuliffe, Joseph R. "Landscape Evolution, Soil Formation, and Ecological Patterns and Processes in Sonoran Desert Bajadas." *Ecological Monographs*, vol. 64, no. 2, The Ecological Society of America, 1994, pp. 112–48.

McHugh, T.A., Morrissey, E.M., Reed, S.C., Hungate, B.A., and Schwartz, E. (2015) Water from air: an overlooked source of moisture in arid and semiarid regions. *Scientific Reports* **5**: 13767.

Mudrak, E.L., Schafer, J.L., Fuentes-Ramirez, A., Holzapfel, C., and Moloney, K.A. (2014) Predictive modeling of spatial patterns of soil nutrients related to fertility islands. *Landscape Ecol* **29**: 491–505.

Ouyang, Hailong, and Chunxiang Hu. "Insight into Climate Change from the Carbon Exchange of Biocrusts Utilizing Non-Rainfall Water." *Scientific Reports*, vol. 7, no. 1, NATURE PUBLISHING GROUP, 2017, pp. 2573–13, doi:10.1038/s41598-017-02812-y.

Pedram, S., Wang, X., Liu, T., and Duan, L. (2018) Simulated dynamics of soil water and pore vapor in a semiarid sandy ecosystem. *Journal of Arid Environments* **151**: 58–82.

Plaza, C., Zaccone, C., Sawicka, K., Méndez, A.M., Tarquis, A., Gascó, G., et al. (2018) Soil resources and element stocks in drylands to face global issues. *Scientific Reports* **8**: 13788.

Prăvălie, Remus. "Drylands Extent and Environmental Issues. A Global Approach." *Earth-Science Reviews*, vol. 161, Elsevier B.V, 2016, pp. 259–78, https://doi.org/10.1016/j.earscirev.2016.08.003.

Poulter, B., Frank, D., Ciais, P., Myneni, R.B., Andela, N., Bi, J., et al. (2014) Contribution of semi-arid ecosystems to interannual variability of the global carbon cycle. *Nature* **509**: 600–603.

Ramond, J.-B., Woodborne, S., Hall, G., Seely, M., and Cowan, D.A. (2018) Namib Desert primary productivity is driven by cryptic microbial community N-fixation. *Sci Rep* **8**: 6921.

Rossel, V., et al. "Proximal Soil Sensing. An Effective Approach for Soil Measurements in Space and Time." *Advances in Agronomy*, vol. 113, 2011, pp. 237–82, doi:10.1016/B978-0-12-386473-4.00010-5.

Safriel, U., Adeel, Z., Niemeijer, D., Puigdefabregas, J., White, R., Lal, R., et al. (2005) Dryland systems. *Ecosystems and Human Well-being: Current State and Trends: Findings of the Condition and Trends Working Group* 623–662.

Scherer, H.W. (2001) Sulphur in crop production — invited paper. *European Journal of Agronomy* **14**: 81–111.

Sentelhas, Paulo C., et al. "Suitability of Relative Humidity as an Estimator of Leaf Wetness Duration." *Agricultural and Forest Meteorology*, vol. 148, no. 3, Elsevier B.V, 2008, pp. 392–400, doi: 10.1016/j.agrformet.2007.09.011.

Shreve, Forrest, and Ira L. Wiggins. *Vegetation and Flora of the Sonoran Desert*. Stanford University Press, 1964.

The Math Works, Inc. MATLAB. Version R2019b, The Math Works, Inc., 2020. Computer Software. www.mathworks.com/.

Throop, H.L. and Archer, S.R. (2008) Shrub (Prosopis velutina) encroachment in a semidesert grassland: spatial–temporal changes in soil organic carbon and nitrogen pools. *Global Change Biology* **14**: 2420–2431.

Uclés, O., et al. "Microlysimeter Station for Long Term Non-Rainfall Water Input and Evaporation Studies." *Agricultural and Forest Meteorology*, vol. 182-183, Elsevier B.V, 2013, pp. 13–20, doi: 10.1016/j.agrformet.2013.07.017.

Wang, C., Wang, X., Liu, D., Wu, H., Lü, X., Fang, Y., et al. (2014) Aridity threshold in controlling ecosystem nitrogen cycling in arid and semi-arid grasslands. *Nature Communications* **5**: 4799.

Wang, L., Kaseke, K.F., and Seely, M.K. (2017) Effects of non-rainfall water inputs on ecosystem functions. *WIREs Water* **4**: e1179.

Wertin, T.M., Young, K., and Reed, S.C. (2018) Spatially explicit patterns in a dryland's soil respiration and relationships with climate, whole plant photosynthesis and soil fertility. *Oikos* **127**: 1280–1290.

Zerger, A., et al. "Environmental Sensor Networks for Vegetation, Animal and Soil Sciences." *International Journal of Applied Earth Observation and Geoinformation*, vol. 12, no. 5, Elsevier, 2010, pp. 303–16, doi: 10.1016/j.jag.2010.05.001.

APPENDIX A

CELL COUNTS FROM THE DBG AND SRER

The heterogeneity of soil microclimates in dryland regions likely has great impact on the microbial populations that live there. Therefore, some preliminary research was performed on the microbial populations of soils from bare and canopy-covered samples from both the DBG and SRER to determine what differences there were between the two sites and their own microclimates.

Cell counts were performed in triplicate on soil samples from both sites. These counts were performed to calculate the cells/g of each soil sample. Cells/g was chosen as a metric over cells/ml to represent the impact of any differences more accurately in compaction, soil grain size and soil composition differences. Samples were taken from beneath a tree canopy or shrub canopy and nearby bare plots at the SRER and DBG, respectively. Samples were fixed in ~2% PFA overnight at 4°C. Fixed cell count samples were centrifuged for 15 min at 4500xg and resuspended in 1x PBS. Samples were left overnight then centrifuged again for 15 min at 4500xg and resuspended in 1x PBS. Samples were washed twice more in PBS for 15 min each. Samples were then resuspended in 1:1 ethanol-PBS and stored at 4°C.

To begin the separation, samples were centrifuged for 15 min at 4500xg and the supernatant was carefully poured off. Sample tubes were then weighed, and each sample were portioned into 2 ml microcentrifuge tubes before being weighed again. 400 µL of 2.5% NaCl was added to each sample tube, then 50 µL detergent mix (100 mM EDTA, 100 mM sodium pyrophosphate, and 1% Tween 80 [v/v]) and 50 µL methanol were added to each. Negative controls were made with just the 2.5% NaCl, methanol and detergent mix. Each sample was vortexed for 15 min at max speed (3200 rpm) and the resulting solutions were sonicated on ice at 282 W/cm^2 pulsing on and off for 20 sec in 2 second increments. Two high-density solutions of Nycodenz were prepared in deionized water to densities of 1.16 g/cm^3 and 1.27 g/cm^3. To create high density gradients for each sample, 2 ml of the 1.27 g/cm^3 solution was pipetted into a 15 ml tube then 2 ml of the 1.16 g/cm^3 Nycodenz solution was carefully layered on top. Samples were then carefully layered onto individual density gradients with a wide gauge needle and centrifuged at 4500xg at 4°C for 90 min. The cell-containing layer was then removed from the density gradient, diluted 1:20 or 1:100, and then filtered. Filters were then stained with 400 µL of 5ug/ml DAPI for 15 min and washed 3x with 5ml of 1x PBS. Filters were then mounted on slides with filtered 2:1 citifluor to TE buffer and imaged. Cells were directly counted using a reticle grid measuring 250 μm^2 in multiple different fields of view (FOV) per sample. The average of these counts was calculated and the number of cells per filter was calculated by comparing the size of the reticle grid to the size of the filter and applying that ratio to the average count. Cells/g were calculated by taking the ratio of cells to grams of soil per sample.

The cell count data (Figure 20) indicates that the locations underneath shrub canopies provided an environment where more microbes could grow. This could be because of the 'island of fertility' effect creating a larger pool of C and N (Mudrak *et al*. 2014) and the tendency for litter to collect beneath these canopies (Throop and Belnap 2019), but it could also be due to shade of the canopies creating slightly more temperate microclimates with lower T and higher RH. The difference in cells density at the SRER and DBG may also be explained by the climate at both sites. The SRER is a semi-arid site, characterized by higher precipitation, overall lower T and higher RH than the arid

DBG site. This difference in climate seems to be represented by the lower cell counts at the DBG regardless of sample location.

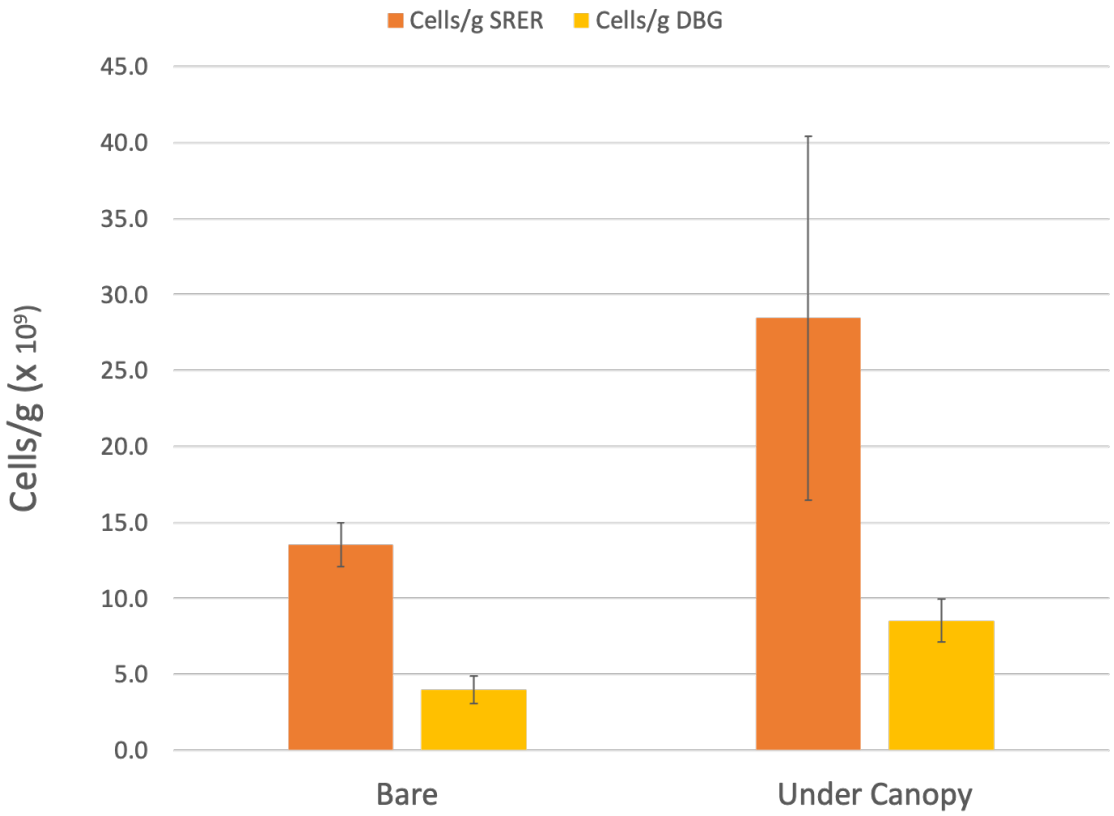

Figure 20: Microbial cell counts of samples from the SRER and DBG sites. Samples were collected from both bare, uncovered areas and under canopy locations. Under canopy locations were taken from beneath creosote bush at the DBG and mesquite canopies at the SRER.

APPENDIX B

LABORATORY HUMIDITY MANIPULATIONS AND CORE SET UP

To test the ability of the AM2315 Relative Humidity and Temperature sensor's ability to measure soil RH, to observe the effect of larger direct wetting events on soil RH, and to test how rapidly elevated RH could impact soil RH, two experiments were performed on soil cores.

First a soil core was dried at 60°C over 3 days and three AM2315 sensors emplaced at increasing depths: 0-2 cm, 2-4 cm and 4-6 cm. The surface of the soil core was wet to saturation, ~ 18 ml water, and the drying process was observed 6 days at room temperature. Immediately, the sensors at 0-2 cm depth and 2-4 cm depth increased in RH rapidly with the surface sensor reaching a maximum of 82% RH within 5 hours and the mid-depth core reaching a maximum relative humidity of 42% RH within 30 hours (Figure 21). The deepest sensor did not experience an increase in RH until 51 hours following the direct wetting event and eventually stabilized at a RH of ~12%, 133 hours following the direct wetting event.

As depth increases, the data indicates it takes longer for soil RH to reach its maximum value as a result of a wetting event. In particular, the data suggests that a greater than 4 cm depth for sensor placement for these soil cores will not see a change in soil RH from a large wetting event for more than 2 days. As a result of this experiment,

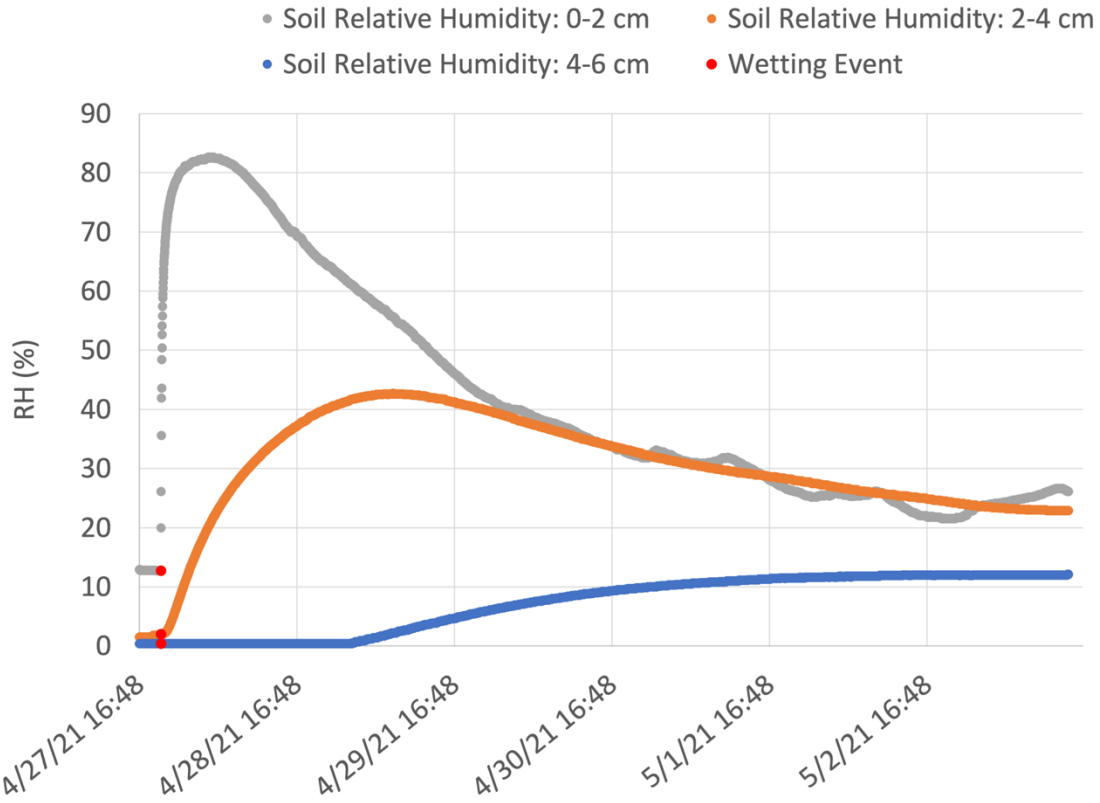

Figure 21: Soil core soil RH response to direct surface wetting at varying depths: 0-2 cm (Gray), 2-4 cm (Orange), and 4-6 cm (Blue). Three AM2315 sensors were placed in the soil core, one at each depth. Cores were wetted until surface reached saturation, ~ 18 ml, and allowed to dry at room temperature.

RH sensors for smaller wetting event experiments and humidity manipulations which could reasonably be assumed to have smaller, less penetrative changes in humidity did not include sensors below 4 cm depth.

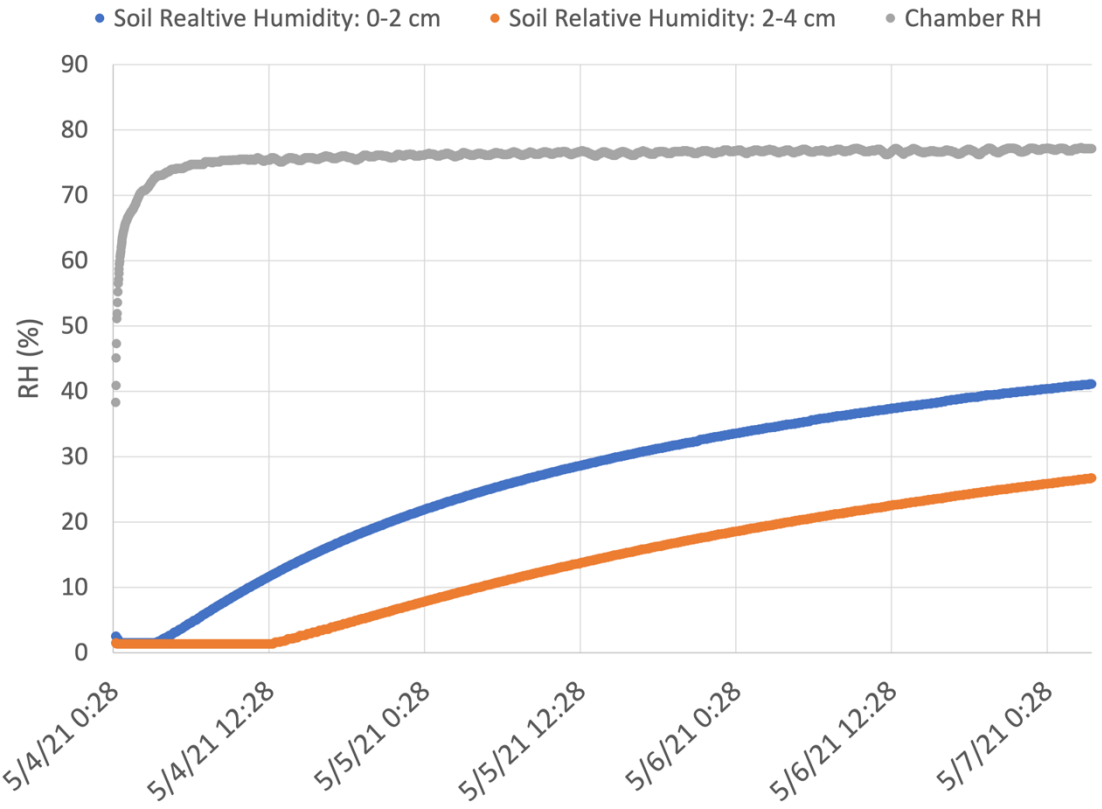

Figure 22: Soil core soil RH response to humidity manipulation in a 75% humidity chamber. Two AM2315 sensors were emplaced at 0-2 cm depth (Blue) and 2-4 cm depth (Orange). The soil core was then placed in an NaCl-based humidity chamber and soil RH response was observed at room temperature.

To determine if and to what extent elevated atmospheric RH could increase soil RH, another soil core was dried as described above and prepared with 2 AM2315 sensors at 0-2 cm depth and 2-4 cm depth. This core was then placed in a 75% NaCl-based humidity chamber and observed over the course of 3 days.

While the humidity chamber was, prior to the experiment, kept at 75% RH, opening the chamber to place the core caused the chamber's humidity to drop. The chamber took ~ 3 hours to regenerate to 75% RH. Following the core's placement in the humidity chamber, the surface sensor began to read increases in soil RH within 4 hours (1 hour since the humidity chamber had returned to 75% RH) (Figure 22). The deeper sensor began reading increases in soil RH within 12 hours of elevated humidity (9 hours since the humidity chamber had returned to 75% RH). Once soil RH began increasing, both sensors saw increases in soil RH until the experiment ended.

In conjunction with the prior direct wetting experiment, the data from these RH manipulations indicates that surface soil RH is most rapidly impacted by both direct wetting and elevated humidities. While this is somewhat unsurprising, it is important to consider that the data indicates that deeper RH and moisture sensors may not see input from elevated RH or even direct wetting events until long periods of time have passed. Especially since the liquid water input from NRM events is likely to be small, it is very possible that events will not last for long enough durations for deeper sensors to see them. Furthermore, in field settings, particularly during higher temperature seasons, evaporation may play a greater role than in these room temperature experiments and further increase the length of time it takes for deeper sensors to see moisture input from elevated RH or NRM events.

APPENDIX C

SOIL RELATIVE HUMIDITY EVENTS BY DURATION AND DEPTH

To determine if the duration of elevated RH events (> 75% RH) was impacting the VSWC measured by the NEON soil moisture sensors at a depth of 6 cm at the SRER, the NEON data analyzed in Figure 10 were assessed to plot event duration as well (Figure 23). These data indicated that, while the majority of events were below 10 hours in duration, those events where relative humidity was consistently high for durations longer that 10 hours seemed to also be correlated with increased scatter in ΔVSWC, particularly at humidities above 90%.

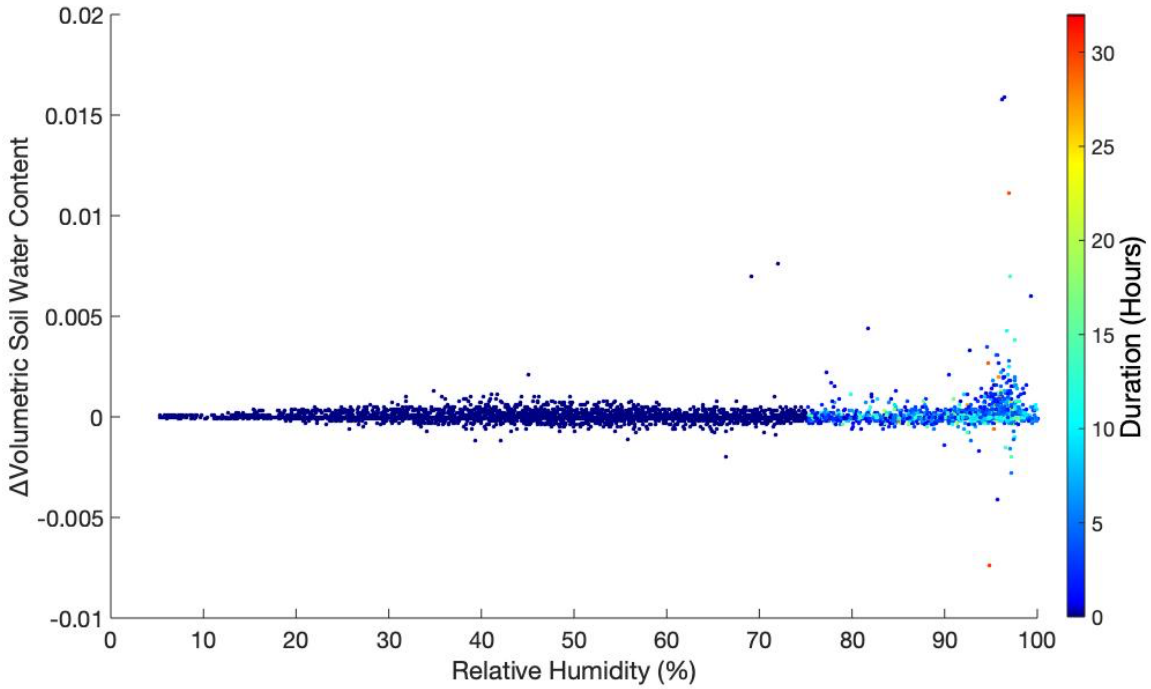

Figure 23: The duration of elevated RH events (>75%) when comparing ΔVSWC against RH at the SRER from Jul. 2018 – Aug. 2020 as described in Figure 10. Individual points represent a 30-min period. The duration of the elevated RH event prior to each point is indicated by color.

To determine the frequency of elevated humidity event durations lasting long enough to impact soil moisture sensors, a coupled analyses of laboratory data on soil moisture collected in Appendix B and the SRER RH data from Jul. 2018 – Aug. 2020 analyzed in Chapter 2 was performed (Figure 24). This data indicated that most elevated RH events would impact measured soil moisture by probes at depths ranging from 0-4 cm. However, no events lasted long enough that soil moisture sensors at depths >4 cm would see appreciable increases in soil moisture as indicated by Figures 21 and 22.

These analyses provide further evidence that future work, research campaigns, and ESNs should emplace shallower soil moisture sensors to accurately measure the changes in soil moisture due to NRM events.

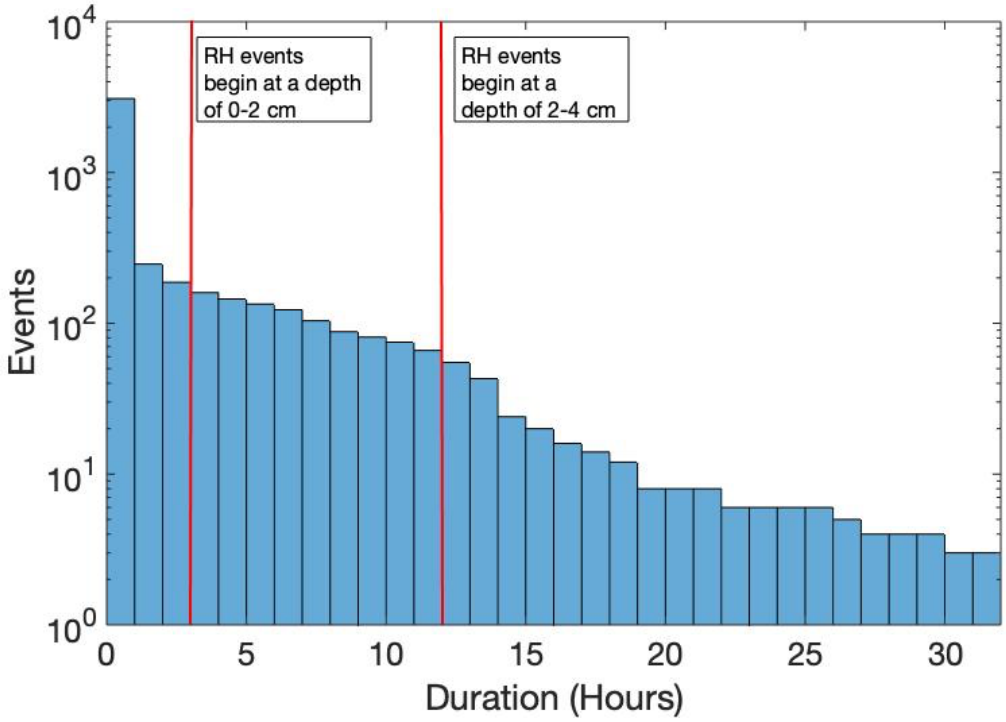

Figure 24: The frequency of durations of contiguous elevated RH events (>75%) at the SRER from Jul. 2018 – Aug. 2020. Each event indicates a 30-minute contiguous period of elevated humidity. Red lines indicate the duration of an elevated RH event required for sensors at a given depth to see increases in soil RH as determined in Appendix B and Figure 22. Below a depth of 4 cm, even large soil wetting events mimicking rainfall as in Appendix B, Figure 21 do not see an appreciable increase in soil RH until a 51-hour duration has elapsed.